

PAPER • OPEN ACCESS

A design framework for actively crosslinked filament networks

To cite this article: Sebastian Fürthauer *et al* 2021 *New J. Phys.* **23** 013012

View the [article online](#) for updates and enhancements.



PAPER

A design framework for actively crosslinked filament networks

OPEN ACCESS

RECEIVED
26 August 2020REVISED
7 December 2020ACCEPTED FOR PUBLICATION
11 December 2020PUBLISHED
20 January 2021

Original content from
this work may be used
under the terms of the
[Creative Commons
Attribution 4.0 licence](#).

Any further distribution
of this work must
maintain attribution to
the author(s) and the
title of the work, journal
citation and DOI.

Sebastian Fürthauer^{1,*} , Daniel J Needleman^{1,2} and Michael J Shelley^{1,3} ¹ Center for Computational Biology, Flatiron Institute, New York, NY-10010, United States of America² Paulson School of Engineering & Applied Science and Department of Molecular & Cellular Biology, Harvard University, Cambridge, MA-02138, United States of America³ Courant Institute, New York University, New York, NY-10012, United States of America

* Author to whom any correspondence should be addressed.

E-mail: sfuertbauer@flatironinstitute.org

Keywords: cytoskeleton, polymer networks, active matter, active gels, continuum mechanics

Abstract

Living matter moves, deforms, and organizes itself. In cells this is made possible by networks of polymer filaments and crosslinking molecules that connect filaments to each other and that act as motors to do mechanical work on the network. For the case of highly cross-linked filament networks, we discuss how the material properties of assemblies emerge from the forces exerted by microscopic agents. First, we introduce a phenomenological model that characterizes the forces that crosslink populations exert between filaments. Second, we derive a theory that predicts the material properties of highly crosslinked filament networks, given the crosslinks present. Third, we discuss which properties of crosslinks set the material properties and behavior of highly crosslinked cytoskeletal networks. The work presented here, will enable the better understanding of cytoskeletal mechanics and its molecular underpinnings. This theory is also a first step toward a theory of how molecular perturbations impact cytoskeletal organization, and provides a framework for designing cytoskeletal networks with desirable properties in the lab.

1. Introduction

Materials made from constituents that use energy to move are called active. These inherently out of equilibrium systems have attractive physical properties: active materials can spontaneously form patterns [1], collectively move [2–4], self-organize into structures [5, 6], and do work [7]. Biology, through evolution, has found ways to exploit this potential. The cytoskeleton, an active material made from biopolymer filaments and molecular scale motors, drives cellular functions with remarkable spatial and temporal coordination [8, 9]. The ability of cells to move, divide, and deform relies on this robust, dynamic and adaptive material. To understand the molecular underpinnings of cellular mechanics and design similarly useful active matter systems in the lab, a theory that predicts their behavior from the interactions between their constituents is needed. The aim of this paper, is to address this challenge for highly crosslinked systems made from rigid rod-like filaments and molecular scale motors.

The large-scale physics of active materials can be described by phenomenological theories, which are derived from symmetry considerations and conservation laws, without making assumptions on the detailed molecular scale interactions that give rise to the materials properties [10–12]. This has allowed exploring the exotic properties of active materials, and the quantitative description of subcellular structures, such as the spindle [6, 13] (the structure that segregates chromosomes during cell division) and the cell cortex [14–17] (the structure that provides eukaryotic cells with the ability to control their shape), even though the microscale processes at work often remain opaque. In contrast, understanding how molecular perturbations affect cellular scale structures requires theories that explain how material properties depend on the underlying molecular behaviors. Designing active materials with desirable properties in the lab will also require the ability to predict how emergent properties of materials result from their constituents [18]. Until now, the attempts to bridge this gap have relied heavily on computational methods [19–21], or were restricted to sparsely crosslinked systems [22–26], one dimensional systems [27, 28], or systems with

permanent crosslinks [29]. Our interest here are cytoskeletal networks, which are in general highly crosslinked by tens to hundreds of transient crosslinks linking each filament into the network. In this regime, the forces generated by different crosslinks in the network balance against each other, and not against friction with the surrounding medium, as they would in a sparsely crosslinked regime [30].

We derive how the large scale properties of an actively crosslinked network of cytoskeletal filaments depend on the micro-scale interactions between its components. This theory generalizes our earlier work on one specific type of motor-filament mixture, XCTK2 and microtubules [30, 31], by introducing a generic phenomenological model to describe the forces that crosslink populations exert between filaments.

The structure of this paper is as follows. In section 2, we discuss the force and torque balance for systems of interacting particles, and specialize to the case of interacting rod-like filaments. This will allow us to introduce key concepts of the continuum description, such as the network stress tensor. Next, in section 3, we present a phenomenological model for crosslink interactions between filaments, that can describe the properties of many different types of crosslinks in terms of just a few parameters, which we call crosslink moments. In section 4, we derive the continuum theory for highly crosslinked active networks and obtain the equations of motion for these systems. Finally, in section 5 we give an overview of the main predictions of our theory and discuss the consequences of specific micro-scale properties for the mechanical properties of the consequent active material. We summarize and contextualize our findings in the discussion section 6.

2. Force and torque balance in systems of interacting rod-like particles

We start by discussing the generic framework of our description. In this section we give equations for particle, momentum and angular momentum conservation and introduce the stress tensor, for generic systems of particles with short ranged interactions. We then specialize to the case of interacting rod-like filaments, which form the networks that we study here.

2.1. Particle number continuity

Consider a material that consists of a large number N of particles, that are characterized by their center of mass positions \mathbf{x}_i and their orientations \mathbf{p}_i , where $|\mathbf{p}_i| = 1$ is a unit vector and i is the particle index. Here and in the following we will use bold-faced symbols to denote vectors. In some cases we will also use capitalized bold symbol to denote a tensor but it will be clear in context. For clarity we define all vector and tensor operations in appendix A in terms of index notation. We define the particle number density

$$\psi(\mathbf{x}, \mathbf{p}) = \sum_i \delta(\mathbf{x} - \mathbf{x}_i) \delta(\mathbf{p} - \mathbf{p}_i). \quad (1)$$

Here and in the following $\delta(\mathbf{x} - \mathbf{x}_i)$ has dimensions of inverse volume, while $\delta(\mathbf{p} - \mathbf{p}_i)$ is dimensionless. Also note that, with definition equation (1), $\psi(\mathbf{x}, \mathbf{p})$ is a distribution and not a continuous function. However, a continuous density function can easily be obtained from the density distribution by averaging over a coarse graining volume, see appendix B, and all results defined here for the distribution equally hold for the function. Thus, in the following, we will use distributions and functions interchangeably, to unburden our notation. Ultimately, our goal is to predict how ψ changes over time. This is given by the Smoluchowski equation

$$\partial_t \psi(\mathbf{x}, \mathbf{p}) = -\nabla \cdot (\dot{\mathbf{x}}\psi) - \partial_{\mathbf{p}} \cdot (\dot{\mathbf{p}}\psi), \quad (2)$$

where

$$\dot{\mathbf{x}}\psi = \sum_i \dot{\mathbf{x}}_i \delta(\mathbf{x} - \mathbf{x}_i) \delta(\mathbf{p} - \mathbf{p}_i) \quad (3)$$

and

$$\dot{\mathbf{p}}\psi = \sum_i \dot{\mathbf{p}}_i \delta(\mathbf{x} - \mathbf{x}_i) \delta(\mathbf{p} - \mathbf{p}_i) \quad (4)$$

define $\dot{\mathbf{x}}$ and $\dot{\mathbf{p}}$, the fluxes of particle position and orientation. The aim of this paper is to derive $\dot{\mathbf{x}}$ and $\dot{\mathbf{p}}$, from the forces and torques that act on and between particles.

2.2. Force balance

Each particle in the active network obeys Newton's laws of motion. That is

$$\dot{\mathbf{g}}_i = \sum_j \mathbf{F}_{ij} + \mathbf{F}_i^{(\text{drag})}, \quad (5)$$

where \mathbf{g}_i is the particle momentum, and \mathbf{F}_{ij} is the force that particle j exerts on particle i . Moreover, $\mathbf{F}_i^{(\text{drag})}$ is the drag force between the particle i and the fluid in which it is immersed. Momentum conservation implies

$\mathbf{F}_{ij} = -\mathbf{F}_{ji}$. We are interested in systems where the direct particle–particle interactions are short ranged. This means that $\mathbf{F}_{ij} \neq 0$ only if $|\mathbf{x}_i - \mathbf{x}_j| < d$, where d is an interaction length that is small (relative to system size).

The momentum density is defined by

$$\mathbf{g} = \sum_i \delta(\mathbf{x} - \mathbf{x}_i) \mathbf{g}_i \quad (6)$$

which, using equation (5), obeys

$$\partial_t \mathbf{g} + \nabla \cdot \sum_i \delta(\mathbf{x} - \mathbf{x}_i) \mathbf{v}_i \mathbf{g}_i = \sum_{ij} \delta(\mathbf{x} - \mathbf{x}_i) \mathbf{F}_{ij} + \sum_i \delta(\mathbf{x} - \mathbf{x}_i) \mathbf{F}_i^{(\text{drag})}, \quad (7)$$

where $\mathbf{v}_i = \dot{\mathbf{x}}_i$ is the velocity of the i th particle. Note also that $\mathbf{v}_i \mathbf{g}_i$ denotes an outer product and is a second rank tensor, see appendix A. The terms on the left-hand side of equation (7) are inertial, and in the overdamped limit, relevant to the systems studied here, they are vanishingly small. Interactions between particles are described by the first term on the right-hand side of equation (7) and generate a momentum density flux Σ (the stress tensor) through the material. Using that d is small, so that particle–particle interactions are short-ranged, gives

$$\begin{aligned} \sum_{ij} \delta(\mathbf{x} - \mathbf{x}_i) \mathbf{F}_{ij} &= \frac{1}{2} \sum_{ij} (\delta(\mathbf{x} - \mathbf{x}_i) - \delta(\mathbf{x} - \mathbf{x}_j)) \mathbf{F}_{ij} \\ &= -\nabla \cdot \sum_{ij} \delta(\mathbf{x} - \mathbf{x}_i) \frac{\mathbf{x}_i - \mathbf{x}_j}{2} \mathbf{F}_{ij} + \mathcal{O}(d^3) \\ &= \nabla \cdot \Sigma. \end{aligned} \quad (8)$$

where

$$\Sigma = -\sum_{ij} \delta(\mathbf{x} - \mathbf{x}_i) \frac{\mathbf{x}_i - \mathbf{x}_j}{2} \mathbf{F}_{ij} + \mathcal{O}(d^3). \quad (9)$$

Note that equation (9) does not necessarily produce a symmetric stress tensor. Force couples for which \mathbf{F}_{ij} and $\mathbf{x}_i - \mathbf{x}_j$ are not parallel generate antisymmetric stress contributions, since these couples are not torque free. We discuss how to reconcile this with angular momentum conservation in appendix E. The drag force density is

$$\mathbf{f} = \sum_i \delta(\mathbf{x} - \mathbf{x}_i) \mathbf{F}_i^{(\text{drag})}, \quad (10)$$

and after dropping inertial terms, the force balance reads

$$\nabla \cdot \Sigma + \mathbf{f} = \mathbf{0}, \quad (11)$$

and the total force on particle i obeys

$$\sum_j \mathbf{F}_{ij} + \mathbf{F}_i^{(\text{drag})} = \mathbf{0}. \quad (12)$$

This completes the discussion of the force balance of the system. We next discuss angular momentum conservation.

2.3. Torque balance

The total angular momentum of particle i , is given by

$$\ell_i^{(\text{tot})} = \ell_i + \mathbf{x}_i \times \mathbf{g}_i, \quad (13)$$

and is conserved, where ℓ_i is its spin angular momentum and its $\mathbf{x}_i \times \mathbf{g}_i$ its orbital angular momentum. Newton's laws imply that

$$\dot{\ell}_i = \sum_j \mathbf{T}_{ij} + \mathbf{T}_i^{(\text{drag})}, \quad (14)$$

where \mathbf{T}_{ij} is the torque exerted by particle j on particle i , in the frame of reference moving with particle i , and $\mathbf{T}_i^{(\text{drag})}$ is the torque from interaction with the medium, in the same frame of reference. Importantly, since the total angular momentum is a conserved quantity, the total torque transmitted between particles

$\mathbf{T}_{ij} + \mathbf{x}_i \times \mathbf{F}_{ij} = -\mathbf{T}_{ji} - \mathbf{x}_j \times \mathbf{F}_{ji}$ is odd upon exchange of the particle indices i and j . Taking a time derivative of equation (13) and using equation (5) leads to the torque balance equation for particle i

$$\sum_j (\mathbf{T}_{ij} + \mathbf{x}_i \times \mathbf{F}_{ij}) + \mathbf{T}_i^{(\text{drag})} + \mathbf{x}_i \times \mathbf{F}_i^{(\text{drag})} = \mathbf{0}, \quad (15)$$

and thus

$$\sum_j \mathbf{T}_{ij} + \mathbf{T}_i^{(\text{drag})} = \mathbf{0}, \quad (16)$$

where we ignored the inertial term $\mathbf{v}_i \times \mathbf{g}_i$ and used equation (12). The angular momentum fluxes associated with spin, orbital and total angular momentum are discussed in appendix E for completeness.

2.4. The special case of rod-like filaments

We now specialize to rod-like particles, such as the microtubules and actin filaments that make up the cytoskeleton. In particular, we calculate the objects \mathbf{F}_{ij} , \mathbf{T}_{ij} , and Σ from prescribed interaction forces and torques along rod-like particles.

2.4.1. Forces

Again, filament i is described by its center of mass \mathbf{x}_i and orientation vector \mathbf{p}_i . All filaments are taken as having the same length L , and position along filament i is given by $\mathbf{x}_i + s_i \mathbf{p}_i$, where $s_i \in [-L/2, L/2]$ is the signed arclength. We consider the vectorial momentum flux from arclength position s_i on filament i to arclength position s_j on filament j

$$\mathbf{f}_{ij} = \mathbf{f}_{ij}(s_i, s_j), \quad (17)$$

where $\mathbf{f}_{ij} = -\mathbf{f}_{ji}$ and having dimensions of force over area, i.e. a stress. Here we focus on forces generated by crosslinks; see figure 1(a). The total force between two particles is

$$\mathbf{F}_{ij} = \left[\delta(\mathbf{x} - \mathbf{x}_j - s_j \mathbf{p}_j) \mathbf{f}_{ij} \right]_{\Omega(\mathbf{x}_i + s_i \mathbf{p}_i)}^{ij}, \quad (18)$$

where the brackets $[\dots]_{\Omega(\mathbf{x}_i)}^{ij}$ denote the operation

$$[\phi]_{\Omega(\mathbf{x}_i)}^{ij} = \int_{-\frac{L}{2}}^{\frac{L}{2}} ds_i \int_{-\frac{L}{2}}^{\frac{L}{2}} ds_j \int_{\Omega(\mathbf{x}_i)} d\mathbf{x}^3 \phi, \quad (19)$$

where ϕ is a dummy argument and Ω is a sphere whose radius is the size of a cross-linker (i.e., d , the interaction distance). With the definition equation (19), the operation $[\dots]_{\Omega(\mathbf{x}_i + s_i \mathbf{p}_i)}^{ij}$ integrates its argument over all geometrically possible crosslink interactions, between filaments i and j ; see figure 1(b). By Taylor expanding and keeping terms up to second order in the filament arc length (s_i, s_j), we find

$$\mathbf{F}_i^{(\text{tot})} = \sum_j \left[\left\{ \begin{array}{l} 1 \\ + (s_i \mathbf{p}_i - s_j \mathbf{p}_j) \cdot \nabla \\ + \frac{1}{2} (s_i^2 \mathbf{p}_i \mathbf{p}_i + s_j^2 \mathbf{p}_j \mathbf{p}_j) : \nabla \nabla \end{array} \right\} \delta(\mathbf{x} - \mathbf{x}_j) \mathbf{f}_{ij} \right]_{\Omega(\mathbf{x}_i)}^{ij} + \mathbf{F}_i^{(\text{drag})} \quad (20)$$

and the network stress

$$\Sigma = -\frac{1}{2} \sum_{i,j} \left[\left(\frac{\delta(\mathbf{x} - \mathbf{x}_i) \delta(\mathbf{x}' - \mathbf{x}_j)}{(\mathbf{x}_i - \mathbf{x}_j + s_i \mathbf{p}_i - s_j \mathbf{p}_j)} \right) \mathbf{f}_{ij} \right]_{\Omega(\mathbf{x}_i)}^{ij}, \quad (21)$$

where we used that $\mathbf{f}_{ij} = -\mathbf{f}_{ji}$.

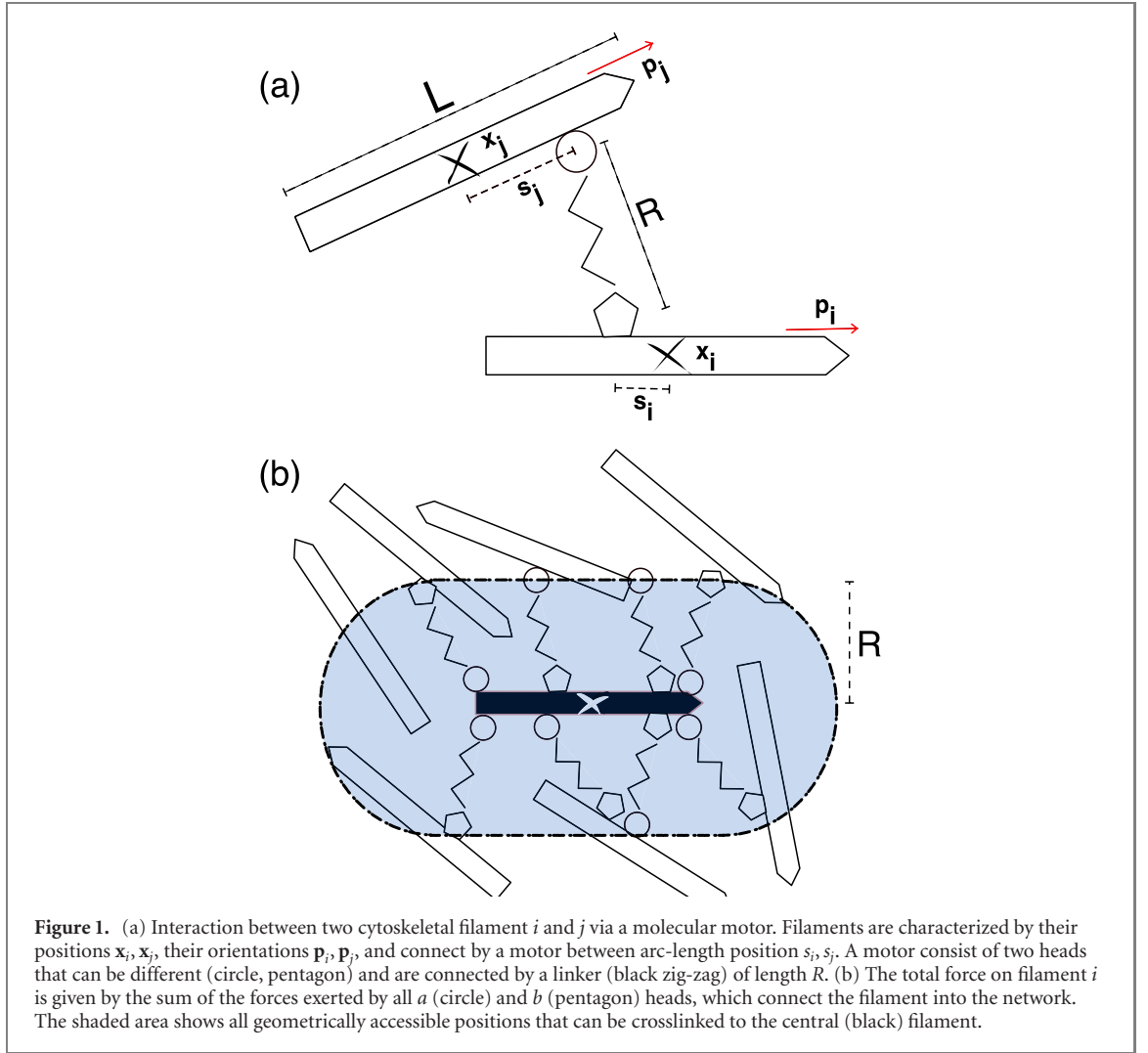
2.4.2. Torques

Similarly, the angular momentum flux that crosslinkers exert between filaments can be written as

$$\mathbf{t}_{ij} = \bar{\mathbf{t}}_{ij}(s_i, s_j) + s_i \mathbf{p}_i \times \mathbf{f}_{ij}, \quad (22)$$

which dimensionally is a torque per unit area. Thus

$$\mathbf{T}_{ij} = [\delta(\mathbf{x} - \mathbf{x}_j - s_j \mathbf{p}_j) \mathbf{t}_{ij}]_{\Omega(\mathbf{x}_i + s_i \mathbf{p}_i)}^{ij} \quad (23)$$



which leads to

$$\mathbf{T}_i^{(\text{tot})} = \mathbf{T}_i^{(\text{drag})} + \sum_j \left[\begin{array}{l} \delta(\mathbf{x} - \mathbf{x}_j) (\bar{\mathbf{t}}_{ij} + s_i \mathbf{p}_i \times \mathbf{f}_{ij}) \\ + (s_i \mathbf{p}_i - s_j \mathbf{p}_j) \cdot \nabla \delta(\mathbf{x} - \mathbf{x}_j) (\bar{\mathbf{t}}_{ij} + s_i \mathbf{p}_i \times \mathbf{f}_{ij}) \\ + \frac{1}{2} (s_i^2 \mathbf{p}_i \mathbf{p}_i + s_j^2 \mathbf{p}_j \mathbf{p}_j) : \nabla \nabla \delta(\mathbf{x} - \mathbf{x}_j) \bar{\mathbf{t}}_{ij} \end{array} \right]_{\Omega(\mathbf{x}_i)}^{ij}. \quad (24)$$

In the following we will consider crosslinks for which $\bar{\mathbf{t}}_{ij} = 0$, for simplicity.

3. Filament–filament interactions by crosslinks and collisions

We next discuss how filaments in highly crosslinked networks exchange linear and angular momentum. Two types of interactions are important here: interactions mediated by crosslinking molecules, which can be simple static linkers or active molecular motors, and steric interactions. We start by discussing the former.

3.1. Crosslinking interactions

To describe crosslinking interactions, we propose a phenomenological model for the stress \mathbf{f}_{ij} that crosslinkers exert between the attachment positions s_i and s_j on filaments i and j .

$$\begin{aligned} \mathbf{f}_{ij} = & K(s_i, s_j, t) \left(\mathbf{x}_i + s_i \mathbf{p}_i - \mathbf{x}_j - s_j \mathbf{p}_j \right) \\ & + \gamma(s_i, s_j, t) \left(\mathbf{v}_i + s_i \dot{\mathbf{p}}_i - \mathbf{v}_j - s_j \dot{\mathbf{p}}_j \right) \\ & + \left[\sigma(s_i, s_j, t) \mathbf{p}_i - \sigma(s_j, s_i, t) \mathbf{p}_j \right]. \end{aligned} \quad (25)$$

The first term in this model, with coefficient K , is proportional to the displacement between the attachment points, $\mathbf{x}_i + s_i \mathbf{p}_i - \mathbf{x}_j - s_j \mathbf{p}_j$, and captures the effects of crosslink elasticity and motor slow-down under force. The second term, with coefficient γ , is proportional to $\mathbf{v}_i + s_i \dot{\mathbf{p}}_i - \mathbf{v}_j - s_j \dot{\mathbf{p}}_j$, and captures friction-like effects arising from velocity differences between the attachment points. The last terms are motor forces that act along filament orientations \mathbf{p}_i and \mathbf{p}_j , with their coefficients σ having dimensions of stress. Additional forces proportional to the relative rotation rate between filaments, $\dot{\mathbf{p}}_i - \dot{\mathbf{p}}_j$, are allowed by symmetry, but are neglected here for simplicity.

In general, the coefficients K , γ , and σ are tensors that depend on time, the relative orientations between filament i and j and the attachment positions s_i, s_j on both filaments. In this work, we take them to be scalar and independent of the relative orientation, for simplicity. Generalizing the calculations that follow to include the dependences of K , γ and σ on \mathbf{p}_i and \mathbf{p}_j is straightforward but laborious and will be discussed in a subsequent publication. We emphasize that equation (25) is a statement about the expected average effect of crosslinks in a dense local environment and is not a description of individual crosslinking events.

Inserting equation (25) into equations (20), (21) and (24) we find that the stresses and forces collectively generated by crosslinks depend on s_{ij} -moments of the form

$$X_{mm}(\mathbf{x}) = \int_{\Omega(\mathbf{x})} X(s_i, s_j) s_i^n s_j^m \gamma^{ij}, \quad (26)$$

where $X = K$, γ , or σ . We refer to these as crosslink moments. In principle, given equations (20), (21) and (25) only the moments $X_{00}, X_{01}, X_{10}, X_{11}, X_{20}, X_{02}, X_{21}$, and X_{12} , contribute to the stresses and forces in the filament network. We further note that X_{11}, X_{21} and X_{12} are $\mathcal{O}(L^4)$, and can thus be neglected without breaking asymptotic consistency. Moreover, X_{20} and X_{02} can be expressed in terms of lower order moments since $X_{20} = X_{02} + \mathcal{O}(L^4) = (L^2/12)X_{00} + \mathcal{O}(L^4)$.

Finally, by construction $K(s_i, s_j) = K(s_j, s_i)$ and $\gamma(s_i, s_j) = \gamma(s_j, s_i)$, and thus $\gamma_{01} = \gamma_{10} \equiv \gamma_1$ and $K_{01} = K_{10} \equiv K_1$. To further simplify our notation, we introduce $X_0 = X_{00}$. Explicit expressions for the seven crosslinking moments that contribute to the continuum theory are given in the appendix D. There we also discuss how to define crosslink moments for a distribution of filaments with varying length. In summary, in the long wave length limit all forces and stresses in the network can be expressed in terms of just a few moments, $K_0, K_1, \gamma_0, \gamma_1, \sigma_0, \sigma_{01}, \sigma_{10}$. How different crosslinker behavior set these moments will be discussed in section 5.

3.2. Sterically mediated interactions

In addition to crosslinker mediated forces and torques, steric interactions between filaments generate momentum and angular momentum transfer in the system. We model steric interactions by a free energy $E = \int_V e(\mathbf{p}_i, \dots, \mathbf{x}_i, \dots) d^3x$ which depends on all particle positions and orientations. The steric force is

$$\bar{\mathbf{F}}_i = -\frac{\delta E}{\delta \mathbf{x}_i}, \quad (27)$$

and the torque acting on it is

$$\bar{\mathbf{T}}_i = -\frac{\delta E}{\delta \mathbf{p}_i}. \quad (28)$$

This approach is commonly used throughout soft matter physics [32, 33]. Common choices for the free energy density e are the ones proposed by Doi and Edwards [34], or De Gennes and Prost [35].

4. Continuum theory for highly crosslinked active networks

In the previous sections we derived a generic expression for the stresses and forces acting in a network of filaments interacting through local forces and torques, and proposed a phenomenological model for crosslink-driven interactions between filaments. We now combine these two and obtain expressions for the stresses, force, and torques acting in a highly crosslinked filament network, and from there derive equations of motion for the material. We start by introducing the coarse-grain fields in terms of which our theory is phrased.

4.1. Continuous fields

The coarse grained fields of relevance are the number density,

$$\rho = \sum_i \delta(\mathbf{x} - \mathbf{x}_i), \quad (29)$$

the velocity $\mathbf{v} = \langle \mathbf{v}_i \rangle$, the polarity $\mathbf{P} = \langle \mathbf{p}_i \rangle$, the nematic-order tensor $\mathcal{Q} = \langle \mathbf{p}_i \mathbf{p}_i \rangle$, and the third and fourth order tensors $\mathcal{T} = \langle \mathbf{p}_i \mathbf{p}_i \mathbf{p}_i \rangle$, and $\mathcal{S} = \langle \mathbf{p}_i \mathbf{p}_i \mathbf{p}_i \mathbf{p}_i \rangle$. Here the brackets $\langle \cdot \rangle$ signify the averaging operation

$$\rho \langle \phi_i \rangle = \sum_i \delta(\mathbf{x} - \mathbf{x}_i) \phi_i, \quad (30)$$

where ϕ_i is a dummy variable. Furthermore, we define the tensors $\mathbf{j} = \langle \mathbf{p}_i (\mathbf{v}_i - \mathbf{v}) \rangle$, $\mathcal{J} = \langle \mathbf{p}_i \mathbf{p}_i (\mathbf{v}_i - \mathbf{v}) \rangle$, $\mathcal{H} = \langle \mathbf{p}_i \dot{\mathbf{p}}_i \rangle$, and the rotation rate $\omega = \langle \dot{\mathbf{p}}_i \rangle$.

4.2. Stresses

The presence of crosslinkers generates stresses in the material which, through equation (21), depends on the crosslinking force density equation (25). Following the nomenclature from equation (25), we write the material stress as

$$\Sigma = \Sigma^{(K)} + \Sigma^{(\gamma)} + \Sigma^{(V)} + \bar{\Sigma}, \quad (31)$$

where

$$\Sigma^{(K)} = -\rho^2 K_0 \left(\alpha \mathcal{I} + \frac{L^2}{12} \mathcal{Q} \right), \quad (32)$$

is the stress due to the crosslink elasticity,

$$\Sigma^{(\gamma)} = -\rho^2 \left(\eta \nabla \mathbf{v} + \gamma_1 \mathbf{j} + \gamma_0 \frac{L^2}{12} \mathcal{H} \right), \quad (33)$$

is the viscous like stress generated by crosslinkers, and

$$\Sigma^{(V)} = -\rho^2 (\alpha \sigma_0 \nabla \mathbf{P} + \sigma_{10} \mathcal{Q} - \sigma_{01} \mathbf{P} \mathbf{P}) \quad (34)$$

is the stress generated by motor stepping. Here, we defined the network viscosity $\eta = \alpha \gamma_0$ and $\alpha = \frac{3R^2}{10}$.

Finally, the steric (or Ericksen) stress obeys the Gibbs Duhem Relation

$$\nabla \cdot \bar{\Sigma} = \rho \nabla \mu + (\nabla \mathcal{E}) : \mathcal{Q}. \quad (35)$$

where $\mu = -\frac{\delta e}{\delta \rho}$ is the chemical potential, and $\mathcal{E} = -\frac{\delta e}{\delta \mathcal{Q}}$ is the steric distortion field. An explicit definition of $\bar{\Sigma}$ and the derivation of the Gibbs Duhem relation are given in appendix F. Note that for simplicity, we chose that the steric free energy density e depends only on nematic order and not on polarity.

4.3. Forces

We now calculate the forces acting on filament i . The total force \mathbf{F}_i on filament i is given by

$$\mathbf{F}_i = \mathbf{F}_i^{(K)} + \mathbf{F}_i^{(\gamma)} + \mathbf{F}_i^{(V)} + \bar{\mathbf{F}}_i + \mathbf{F}_i^{(\text{drag})}, \quad (36)$$

where

$$\mathbf{F}_i^{(K)} = (\nabla \rho) \cdot \frac{L^2}{12} K_0 (\mathbf{p}_i \mathbf{p}_i - \mathcal{Q}) - \frac{1}{\rho} \nabla \cdot \Sigma^{(K)}, \quad (37)$$

is the elasticity driven force

$$\begin{aligned} \mathbf{F}_i^{(\gamma)} &= \gamma_0 \rho (\mathbf{v}_i - \mathbf{v}) + \gamma_1 \rho (\dot{\mathbf{p}}_i - \omega) \\ &\quad + \gamma_1 (\nabla \rho) \cdot [\mathbf{p}_i (\mathbf{v}_i - \mathbf{v}) - \mathbf{j} - \mathbf{P} (\mathbf{v}_i - \mathbf{v})] \\ &\quad + \frac{L^2}{12} \gamma_0 (\nabla \rho) \cdot [\mathbf{p}_i \dot{\mathbf{p}}_i - \mathcal{H}] \\ &\quad + \frac{L^2}{12} \gamma_0 (\nabla \nabla \rho) : [\mathbf{p}_i \mathbf{p}_i (\mathbf{v}_i - \mathbf{v}) - \mathcal{J} + \mathcal{Q} (\mathbf{v}_i - \mathbf{v})] \\ &\quad - \frac{1}{\rho} \nabla \cdot \Sigma^{(\gamma)}. \end{aligned} \quad (38)$$

is the viscous like force, and

$$\begin{aligned} \mathbf{F}_i^{(V)} &= \rho \sigma_0 (\mathbf{p}_i - \mathbf{P}) \\ &\quad + (\nabla \rho) \cdot [\sigma_{10} (\mathbf{p}_i \mathbf{p}_i - \mathcal{Q}) - \sigma_{01} (\mathbf{p}_i \mathbf{P} + \mathbf{P} \mathbf{p}_i - 2\mathbf{P} \mathbf{P})] \\ &\quad + \frac{L^2}{12} \sigma_0 (\nabla \nabla \rho) : [\mathbf{p}_i \mathbf{p}_i \mathbf{p}_i + \mathcal{Q} \mathbf{p}_i - \mathbf{p}_i \mathbf{p}_i \mathbf{P} - \mathcal{T}] - \frac{1}{\rho} \nabla \cdot \Sigma^{(V)}. \end{aligned} \quad (39)$$

is the motor force. Here we introduced the shorthand: to denote two subsequent inner products, see appendix A. Finally,

$$\bar{\mathbf{F}}_i = -\frac{\nabla \mathcal{E}}{\rho} : (\mathbf{p}_i \mathbf{p}_i - \mathcal{Q}) - \frac{1}{\rho} \nabla \cdot \bar{\boldsymbol{\Sigma}}, \quad (40)$$

is the steric force on filament i , where we again chose e to only depend on nematic order and not on polarity.

4.4. Crosslinker induced torque

We next calculate the torques acting on filament i . The total torque acting on filament i is

$$\mathbf{T}_i = \mathbf{T}_i^{(\gamma)} + \mathbf{T}_i^{(V)} + \bar{\mathbf{T}}_i + \mathbf{T}_i^{(\text{drag})} \quad (41)$$

Note, that crosslinker elasticity does not contribute. Here

$$\begin{aligned} \mathbf{T}_i^{(\gamma)} &= \gamma_1 \rho \mathbf{p}_i \times (\mathbf{v}_i - \mathbf{v}) + \frac{L^2}{12} \gamma_0 \rho \mathbf{p}_i \times \dot{\mathbf{p}}_i \\ &\quad + \frac{L^2}{12} \gamma_0 \mathbf{p}_i \times (\mathbf{p}_i \cdot \nabla \rho) (\mathbf{v}_i - \mathbf{v}) \\ &\quad - \frac{L^2}{12} \gamma_0 \rho \mathbf{p}_i \times (\mathbf{p}_i \cdot \nabla \mathbf{v}) \end{aligned} \quad (42)$$

and

$$\mathbf{T}_i^{(V)} = -\rho \mathbf{p}_i \times \left(\sigma_{01} \mathbf{P} + \frac{L^2}{12} \sigma_0 \mathbf{p}_i \cdot \nabla \mathbf{P} \right) - \frac{L^2}{12} \sigma_0 \mathbf{p}_i \times (\mathbf{p}_i \cdot \nabla \rho) \mathbf{P} \quad (43)$$

are the viscous and motor torques, respectively. Steric interactions contribute to the torque

$$\bar{\mathbf{T}}_i = \mathbf{p}_i \times \frac{\mathcal{E}}{\rho} \cdot \mathbf{p}_i. \quad (44)$$

4.5. Equations of motion

To find equations of motion for the highly crosslinked network, we use equations (36)–(39), and obtain

$$\mathbf{v}_i - \mathbf{v} = -\frac{\sigma_0}{\gamma_0} (\mathbf{p}_i - \mathbf{P}) - \frac{1}{\rho \gamma_0} \left(\mathbf{F}_i^{(\text{drag})} - f/\rho \right) + \mathcal{O}(L^2), \quad (45)$$

which will be a useful low-order approximation to $\mathbf{v}_i - \mathbf{v}$. Note too that we have dropped steric forces, since $\nabla \mathcal{E}/\rho$ scales with the inverse of the system size, which is much larger than L . Using equation (45) in equation (41) we find the equation of motion for filament rotations,

$$\dot{\mathbf{p}}_i = (\mathcal{I} - \mathbf{p}_i \mathbf{p}_i) \cdot \left\{ \begin{array}{l} \frac{\mathbf{p}_i \cdot \mathcal{U}}{12} \\ + \frac{\gamma_0 L^2 \rho^2 \mathbf{p}_i \cdot \mathcal{E}}{\gamma_0 L^2 \rho^2} \\ + \frac{12}{\gamma_0 L^2} A^{(\mathbf{P})} \mathbf{P} \end{array} \right\}, \quad (46)$$

where we neglect drag mediated terms, which are subdominant at high density, for simplicity. A detailed calculation, and expressions which includes drag terms, is given in appendix C. Here,

$$\mathcal{U} = \nabla \mathbf{v} + \frac{\sigma_0}{\gamma_0} \nabla \mathbf{P}, \quad (47)$$

is the active strain rate tensor, which consists of the strain rate and vorticity $\nabla \mathbf{v}$ and an active polar contribution $\nabla \mathbf{P}$. Moreover

$$A^{(\mathbf{P})} = \sigma_{01} - \sigma_0 \frac{\gamma_1}{\gamma_0}. \quad (48)$$

is the polar activity coefficient. The filament velocities are given by

$$\begin{aligned} \mathbf{v}_i - \mathbf{v} &= -\frac{\sigma_0}{\gamma_0} (\mathbf{p}_i - \mathbf{P}) \\ &\quad - \frac{\gamma_1}{\gamma_0} ((\mathbf{p}_i - \mathbf{P}) \cdot \mathcal{U} - (\mathbf{p}_i \mathbf{p}_i \mathbf{p}_i - \mathcal{T}) : \mathcal{U}) \\ &\quad - \frac{12\gamma_1}{L^2 \rho^2 \gamma_0^2} ((\mathbf{p}_i - \mathbf{P}) \cdot \mathcal{E} - (\mathbf{p}_i \mathbf{p}_i \mathbf{p}_i - \mathcal{T}) : \mathcal{E}) + \frac{12\gamma_1}{L^2 \gamma_0^2} A^{(\mathbf{P})} (\mathbf{p}_i \mathbf{p}_i - \mathcal{Q}) \cdot \mathbf{P}, \end{aligned} \quad (49)$$

where we used equations (45) and (46) in equation (36). In equation (49), we ignored terms proportional to density gradients, for simplicity. The full expression is given in appendix C. After some further algebra

(see appendix C), we arrive at an expression for the material stress in terms of the current distribution of filaments,

$$\boldsymbol{\Sigma} = -\rho^2 (\chi : \mathcal{U} + \alpha K_0 \mathcal{I} + A^{(\mathcal{Q})} \mathcal{Q} - A^{(\mathcal{P})} \mathcal{T} \cdot \mathbf{P}) + \boldsymbol{\Sigma}^{(\mathcal{S})}, \quad (50)$$

where

$$\chi_{\alpha\beta\gamma\mu} = \eta \delta_{\alpha\gamma} \delta_{\beta\mu} + \frac{L^2}{12} \gamma_0 (\mathcal{Q}_{\alpha\gamma} \delta_{\beta\mu} - \mathcal{S}_{\alpha\beta\gamma\mu}), \quad (51)$$

is the anisotropic viscosity tensor,

$$A^{(\mathcal{Q})} = \sigma_{10} - \sigma_0 \frac{\gamma_1}{\gamma_0} + \frac{L^2}{12} K_0 \quad (52)$$

is the nematic activity coefficient, and

$$\boldsymbol{\Sigma}_{\alpha\beta}^{(\mathcal{S})} = \bar{\Sigma}_{\alpha\beta} - (\mathcal{Q}_{\alpha\gamma} \delta_{\beta\mu} - \mathcal{S}_{\alpha\beta\gamma\mu}) \mathcal{E}_{\gamma\mu}. \quad (53)$$

is the steric stress tensor. Together equations (2), (46), (49) and (50) define a full kinetic theory for the highly crosslinked active network.

5. Designing materials by choosing crosslinks

Equations (2), (46), (49) and (50) define a full kinetic theory for highly crosslinked active networks. This theory has the same active stresses known from symmetry based theories for active materials [7, 11, 36] and thus can give rise to the same rich phenomenology. Since our framework derives these stresses from microscale properties of the constituents of the material it enables us to make predictions on how the microscopic properties of the network constituents affect its large scale behavior. We first discuss how motor properties set crosslink moments in equation (25). We then study how these crosslink properties impact the large scale properties of the material.

5.1. Tuning crosslink-moments

The coefficients in equation (25) arise from a distribution of active and passive crosslinks that act between filaments. Consider an ensemble of crosslinking molecules, each consisting of two heads a and b , joined by a spring-like linker; see figure (2). For any small volume in an active network, we can count the number densities $\xi_a(s)$, and $\xi_b(s)$ of a and b heads of doubly-bound crosslinks that are attached to a filament at arc-length position s . In an idealized experiment $\xi_a(s)$ and $\xi_b(s)$ could be determined by recording the positions of motor heads on filaments. The number-density $\xi_{ab}(s_i, s_j)$ of a heads at position s_i on microtubule i connected to b heads at position s_j on microtubule j is then given by

$$\xi_{ab}(s_i, s_j) = \frac{\xi_a(s_i) \xi_b(s_j)}{N_b^{(i)}(s_i)}, \quad (54)$$

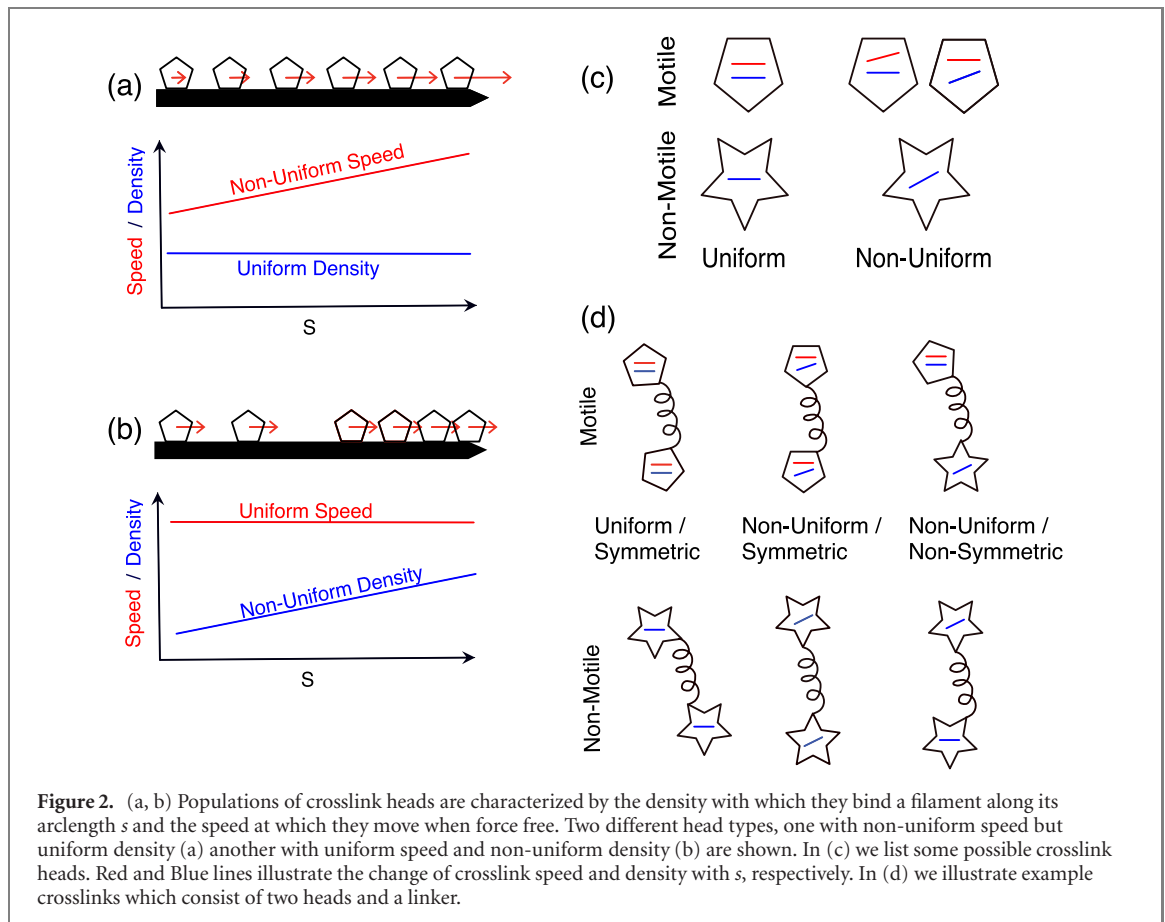
where $N_b^{(i)}(s_i)$ counts the b heads that an a -head attached at position s_i on filament i could be connected to given the crosslink size. It obeys

$$N_b^{(i)}(s_i) = \sum_{k \neq i} \int_{-L/2}^{L/2} ds_k \int_{\Omega(\mathbf{x}_i + s_i \mathbf{p}_i)} d\mathbf{x}^3 \xi_b(s_k) \delta(\mathbf{x}_k + s_k \mathbf{p}_k - \mathbf{x}). \quad (55)$$

Analogous definitions for $\xi_{ba}(s_i, s_j)$ and $N_a^{(i)}(s_i)$ are implied. It follows naturally that $\xi(s_i, s_j) = \xi_{ab}(s_i, s_j) + \xi_{ba}(s_i, s_j)$ is the total number density of crosslinks acting between filaments i and j at the arclength positions s_i, s_j .

Now let $V_a(s), V_b(s)$ be the load-free velocities of motor-heads a, b moving along filaments. Here, $V_a(s), V_b(s)$ are functions of the arc-length position s . Like ξ_a and ξ_b , they are in principle measurable. With these definitions, the force per unit surface that attached motors exert is

$$\begin{aligned} \mathbf{f}_{ij} = & -\Gamma \xi(s_i, s_j) (\mathbf{v}_i + s_i \dot{\mathbf{p}}_i - \mathbf{v}_j + s_j \dot{\mathbf{p}}_j) \\ & - \kappa \xi(s_i, s_j) (\mathbf{x}_i + s_i \mathbf{p}_i - \mathbf{x}_j + s_j \mathbf{p}_j) \\ & - \Gamma ([\xi_{ab}(s_i, s_j) V_a(s_i) + \xi_{ba}(s_i, s_j) V_b(s_i)] \mathbf{p}_i) \\ & + \Gamma ([\xi_{ab}(s_j, s_i) V_a(s_j) + \xi_{ba}(s_j, s_i) V_b(s_j)] \mathbf{p}_j), \end{aligned} \quad (56)$$



where Γ is an effective linear friction coefficient between the two attachment points and κ is an effective spring constant. They depend on the microscopic properties of motors, filaments, and the concentrations of both and their regulators. In general, Γ and κ are second rank tensors, which depend on the relative orientations of filaments. Here we take them to be scalar, for simplicity and consistency with earlier assumptions. By comparing to equation (25) we identify

$$\gamma(s_i, s_j) = -\Gamma \xi(s_i, s_j), \quad (57)$$

$$K(s_i, s_j) = -\kappa \xi(s_i, s_j), \quad (58)$$

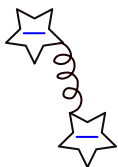
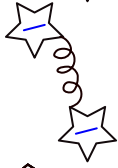
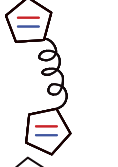
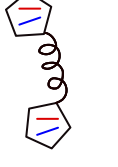
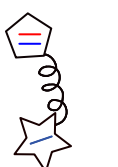
and

$$\sigma(s_i, s_j) = -\Gamma \xi_{ab}(s_i, s_j) V_a(s_i) + \Gamma \xi_{ba}(s_i, s_j) V_b(s_i). \quad (59)$$

Using equations (57)–(59), we now discuss some important classes of crosslinking molecules. We consider crosslinks whose heads can be motile or non-motile, the binding and walking properties can act uniformly or non-uniformly along filaments, and the two heads of the crosslink can be the same (symmetric crosslink) or different (non-symmetric crosslink). Figure 2 maps how varying crosslink types can be constructed, while table 1 lists the moments to which different classes of crosslinks contribute.

Non-motile crosslinks are crosslinks that do not actively move, i.e. $V_a = V_b = 0$. Examples of non-motile crosslinks in cytoskeletal systems are the actin bundlers such as fascin, or microtubule crosslinks such as Ase1 [8]. While these types of crosslinks are not necessarily passive, since the way they binding or unbind can break detailed balance, that their attached heads do not walk along filaments implies that $\sigma_0 = \sigma_{10} = \sigma_{01} = 0$. Non-motile crosslinks change the material properties of the material by contributing to the crosslink moments γ_0, γ_1 and K_0, K_1 . Some non-motile crosslinks bind non-specifically along filaments they interact with, giving uniform distributions. For these $\gamma_1 = K_1 = 0$. Others preferentially associate to filament ends, and thus bind non-uniformly. For these γ_1 and K_1 are positive. Note that the two heads of a non-motile crosslink can be identical (symmetric) or not (non-symmetric). Given the symmetric structure of equations (57) and (58) mechanically a non-symmetric non-motile crosslink behaves the same as a symmetric non-motile crosslink. And *symmetric motor crosslinks* are motor molecules whose two heads have identical properties, i.e. $V_a = V_b = V$ and $\xi_a = \xi_b = \xi$. Examples are the microtubule motor molecule Eg-5 kinesin, and the Kinesin-2 motor construct popularized by many in-vitro experiments [37].

Table 1. Table summarizing which crosslink moments different crosslink types generate.

		γ_0, K_0	γ_1, K_1	σ_0	σ_{10}	σ_{01}
	Symmetric uniform non-motile	Yes	No	No	No	No
	Non-symmetric uniform non-motile	Yes	Yes	No	No	No
	Symmetric uniform motor	Yes	No	Yes	No	No
	Symmetric non-uniform motor	Yes	Yes	Yes	Yes	Yes
	Non-symmetric non-uniform motor	Yes	Yes	Yes	$\sigma_{10} = \sigma_1$	$\sigma_{01} = \sigma_1$

Symmetric motors contribute to the large-scale properties of the material by generating motor forces. In particular they contribute to the crosslink moments σ_0 , σ_{10} , and σ_{01} . From equation (59) it is easy to see that $\sigma_0 = V_0\gamma_0 + V_1\gamma_1/L^2$, where we defined the moments of the motor velocity $V(s_i, s_j)$ using equation (26). Some symmetric motor proteins preferentially associate to filament ends, and display end-clustering behavior, where their walking speed depends on the position at which they are attached to filaments. Motors that do either of these also generate a contribution to σ_{10} and σ_{01} . Since both motor heads are identical we have $\sigma_{10} = \sigma_{01} \equiv \sigma_1$ and from equation (59) we find that $\sigma_1 = \gamma_1 V_0 + V_1\gamma_0$.

Non-symmetric motor crosslinks are motor molecules whose two heads have differing properties. An example is the microtubule-associated motor dynein, that consists of a non-motile end that clusters near microtubule minus-ends and a walking head that binds to nearby microtubules whenever they are within reach [20, 38]. A consequence of motors being non-symmetric is that $\sigma_{10} \neq \sigma_{01}$. Since non-symmetric motors can break the symmetry between the two heads in a variety of ways we spell out the consequences for a few cases. Let us first consider a crosslinker with one head *a* that acts as a passive crosslink ($V_a = 0$) and a second head *b* that acts as a motor, moving with the stepping speed $V_b = V$. For such a crosslink $\sigma_0 = \gamma_0 V_0/2$. If both heads are distributed uniformly along filaments and their V is position independent then $\sigma_{01} = \sigma_{10} = 0$. If the walking *b*-head is distributed nonuniformly ($\xi_b = \xi_b(s)$, $\xi_a = \text{constant}$) then $\sigma_{10} = \gamma_1 V_0$ and $\sigma_{01} = 0$. Conversely, if the static *a*-head has a patterned distribution ($\xi_a = \xi_a(s)$, $\xi_b = \text{constant}$) then $\sigma_{01} = \gamma_1 V_0$, $\sigma_{10} = 0$. Finally, we note that if both heads are distributed uniformly along the filament ($\xi_a = \xi_b = \text{constant}$), but the walking *b*-head of the motor changes its speed as function of position then $\sigma_{10} = V_1\gamma_0/2$ and $\sigma_{01} = 0$.

Note that stresses and forces are additive. Thus it may be possible to design specific crosslink moments by designing mixtures of different crosslinkers. For instance mixing a non-motile crosslink that has specific binding to a filament solution might allow to change just γ_0 and γ_1 in a targeted way. We will elaborate on some of these possibilities in what follows.

5.2. Tuning viscosity

We now discuss how microscopic processes shape the overall magnitude of the viscosity tensor χ . From equation (51) and remembering that $\eta = 3R^2/10\gamma_0$, it is apparent that the overall viscosity of the material is proportional to the number of crosslinking interactions and their resistance to the relative motion of

filaments, quantified by the friction coefficient $\rho^2\gamma_0$. Furthermore, γ_0 itself scales as the squared filament length L , and the cubed crosslink size R (see the definition in appendix D), which, with ρ^2 , sets the overall scale of the viscosity as $\rho^2L^2R^3$.

We next show how micro-scale properties of network constituents shape the anisotropy of χ ; see equation (51). To characterize this we define the anisotropy ratio a as

$$a = \frac{L^2\gamma_0}{12\eta} = \frac{5}{18} \frac{L^2}{R^2}, \quad (60)$$

which is the ratio of the magnitudes of the isotropic part of $\chi_{\alpha\beta\gamma\mu}$, that is $\eta\delta_{\alpha\gamma}\delta_{\beta\mu}$, and its anisotropic part $\gamma_0L^2/12(\mathcal{Q}_{\alpha\gamma}\delta_{\beta\mu} - \mathcal{S}_{\alpha\beta\gamma\mu})$. Most apparently the anisotropy ratio will be large if the typical filament length L is large compared to the motor interaction range R . This is typically the case in microtubule based systems, as microtubules are often microns long and interact via motor groups that are a few tens of nano-meters in scale [8]. Conversely, in actomyosin systems filaments are often shorter (hundreds of nano-meters) and motors-clusters called mini-filaments, can have sizes similar to the filament lengths [8]. The anisotropy of the viscous stress is not exclusive to active systems and has been described before in the context of similar passive systems, such as liquid crystals and liquid crystal polymers [33–35].

5.3. Tuning the active self-strain

The viscous stress in highly crosslinked networks is given by $\chi:\mathcal{U}$, where $\mathcal{U} = \nabla\mathbf{v} + (\sigma_0/\gamma_0)\nabla\mathbf{P}$ takes the role of the strain-rate in passive materials, but with an active contribution $(\sigma_0/\gamma_0)\nabla\mathbf{P}$. Thus, internally driven materials can exhibit active self-straining.

In particular a material in which each filament moves with the velocity $\mathbf{v}_i = -\sigma_0/\gamma_0\mathbf{p}_i + \mathbf{C}$, where \mathbf{C} is a constant vector that sets the net speed of the material in the frame of reference, has $\mathcal{U} = 0$, and thus zero viscous stress. In such a material filaments can slide past each other at a speed σ_0/γ_0 without stressing the material. Notably, the sliding speed is independent of the local polarity and nematic order of the material [30].

The crosslink moments that contribute to the active straining behavior are σ_0 and γ_0 . In active filament networks with a single type of crosslink $\sigma_0/\gamma_0 \simeq V_0$, regardless of crosslink concentration. Thus for single-crosslinker systems, the magnitude of self-straining is independent of the motor concentration [30].

Self-straining can be tuned in mixtures of crosslinks. For instance the addition of a non-motile crosslinker can increase γ_0 , while leaving σ_0 unchanged. In this way self-straining can be relatively suppressed. In table 2 we plot the expected active strain-rate for materials actuated by mixtures of immotile and motor crosslinks. In such a material $\gamma_0 = \gamma_0^{(M)} + \gamma_0^{(X)}$ where $\gamma_0^{(M)}$ denotes the part of γ_0 induced by motile crosslinkers and $\gamma_0^{(X)}$ denotes that from non-motile crosslinkers. The resulting velocity V_{slide} with which a filament slides through the material will scale as $V_{\text{slide}} \simeq \gamma_0^{(M)}/(\gamma_0^{(M)} + \gamma_0^{(X)})$; see table 2.

5.4. Tuning the active pressure

Many active networks spontaneously contract [38] or expand [37]. We now study the motor properties that enable these behaviors.

An active material with stress free boundary conditions, can spontaneously contract if its self-pressure,

$$\Pi = \text{Tr}(\boldsymbol{\Sigma} + \rho^2\chi:\mathcal{U}). \quad (61)$$

is negative. Conversely the material can spontaneously extend if Π is positive. We can also write

$$\Pi = \Pi^{(A)} + \Pi^{(S)}, \quad (62)$$




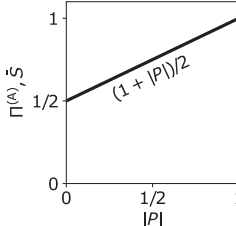
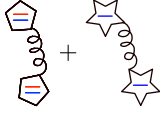
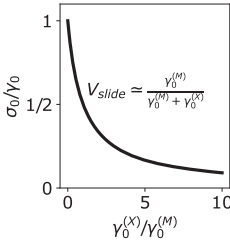
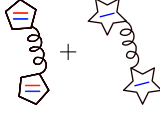
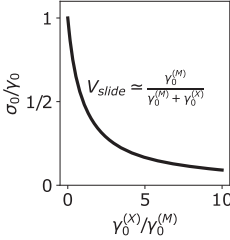
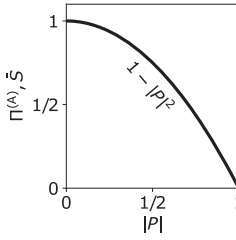
where $\Pi^{(S)} = \text{Tr}(\boldsymbol{\Sigma}^{(S)})$ is the sterically mediated pressure, and $\Pi^{(A)}$ is the activity driven pressure (or active pressure) given by

$$\Pi^{(A)} = -\rho^2(\alpha K_0 + A^{(Q)} - A^{(P)}|\mathbf{P}|^2). \quad (63)$$

see equation (50). Here and in the following we approximated $\text{Tr}(\mathcal{T} \cdot \mathbf{P}) \simeq |\mathbf{P}|^2$ for simplicity. We ask which properties of crosslinks set the active pressure and how its sign can be chosen.

We first discuss how interaction elasticity impacts the active pressure $\Pi^{(A)}$ in the absence of motile crosslinks, i.e. when $\sigma_0 = \sigma_{10} = \sigma_{01} = 0$. In this case, equation (63) simplifies to $\Pi^{(A)} = -\rho^2(\alpha + L^2/12)K_0$, where we used equation (52). Thus, even in the absence of motile crosslinks, active pressure can be generated. This can be tuned by changing the effective spring constant K_0 . We note that $\Pi^{(A)} + \Pi^{(S)} = 0$ when crosslink binding–unbinding obeys detailed balance and the system is in equilibrium. The moment K_0 can have either sign when detailed balance is broken. Microscopically this effect could be achieved, for instance, by a crosslinker in which active processes change the rest length of a spring-like linker between the two heads once they bind to filaments.

Table 2. Active pressure and strain generated by different crosslink types and mixtures. In the plots pertaining to the active strain rate $\gamma_0 = \gamma_0^{(M)} + \gamma_0^{(X)}$ where $\gamma_0^{(M)}$ denotes the part of γ_0 induced by mobile and $\gamma_0^{(X)}$ denotes contribution from non-mobile crosslinkers. The filament sliding velocity expected in a stress free system is $V_{\text{slide}} = \sigma_0/\gamma_0$. Here we normalize it by its maximum. Moreover, $\bar{S} = |\Pi^{(A)}|/q$ is the magnitude of the motor-stepping induced axial stress, i.e. of the axial stress in the limit $K_0 \rightarrow 0$.

Mixture	Active strain, σ_0/γ_0	Active pressure, $\Pi^{(A)}$ axial stress, \bar{S}
	$\frac{\sigma_0}{\gamma_0} = V_0$	No
	$\frac{\sigma_0}{\gamma_0} = V_0$	No
	$\frac{\sigma_0}{\gamma_0} = \frac{V_0^a + V_0^b}{2}$	
		No
		

We next discuss the contributions of motor motility to the active pressure. To start, we study a simplified apolar (i.e. $\mathbf{P} = 0$) system where $K = 0$. In such a system the active pressure is given by

$$\Pi^{(A)} = -\rho^2 \left(\sigma_{10} - \sigma_0 \frac{\gamma_1}{\gamma_0} \right). \quad (64)$$

We ask how motor properties set the value and sign of this parameter combination.

We first point out that generating active pressure by motor stepping requires that either σ_{10} or γ_1 are non-zero. This means that generating active pressure requires breaking the uniformity of binding or walking properties along the filament. A crosslink which has two heads that act uniformly can thus not generate active pressure on its own. However, when operating in conjunction with a passive crosslink that preferentially binds either end of the filament, the same motor can generate an active pressure. This pressure will be contractile if the non-motile crosslinks couple the end that the motor walks toward (γ_1 and σ_0 have the same sign) and extensile if they couple the other (γ_1 and σ_0 have opposite signs). In summary, a motor crosslink that acts the same everywhere along the filaments it couples does not generate active pressure on its own. However, it can do so when mixed with a passive crosslink that acts non-uniformly.

We next ask if a system with just one type of non-uniformly acting crosslink can generate active pressure. To start, consider *symmetric motor crosslinks*, i.e. a motor consisting of two heads with identical (but non-uniform) properties. We then have $\sigma_{01} = \sigma_{10} = \gamma_1 V_0 + \gamma_0 V_1$ and $\sigma_0 = V_0 \gamma_0 + V_1 \gamma_1/L^2$. Using this in equation (64) and dropping the term proportional to γ_1^2 (higher order in this case) we find that such symmetric motor crosslinks generate no contribution to the active pressure when operating alone. However

when operating in concert with a non-motile crosslink, even one that binds filaments uniformly, they can generate an active pressure. The sign of the active pressure is set by the particular asymmetry of motor binding and motion. The system is contractile if motors cluster or speed up near the end toward which they walk, and extensile if they cluster or accelerate near the end that they walk from. Our prediction that many motor molecules can only generate active pressure in the presence of an additional crosslink, might explain observation on acto-myosin gels, which have been shown to contract only when combined a passive crosslink operate in concert with the motor myosin [39].

We next ask if *non-symmetric motor crosslinks* can generate active pressure. Consider a crosslink with one immobile and one walking head. For such a crosslink $\sigma_0 = \gamma_0 V_0/2$. If the immobile head preferentially binds near one filament end, while the walking head attaches everywhere uniformly, then $\sigma_{10} = \gamma_1 V_0$ and $\sigma_{01} = 0$. For such a motor we predict an active pressure proportional to $V_0/2$. The active pressure will be contractile if the static ends bind near the end that the motor head walks to and extensile if the situation is reversed. The motor dynein has been suggested to consist of an immobile head that attaches near microtubule minus ends and a walking head that grabs other microtubules and walks toward their minus ends. Our theory suggests that this should lead to contractions, which is consistent with experimental findings [39].

After having discussed the effects of motor stepping on the active pressure in systems with $\mathbf{P} = 0$, we ask how the situation changes in polar systems. In polar system an additional contribution, $-(\sigma_{01} - \frac{\alpha}{\gamma_0} \sigma_0)|\mathbf{P}|^2$, exists. For symmetric motors, where $\sigma_{01} = \sigma_{10}$ this implies that the active pressure generated by a network of symmetric motors and passive crosslinks is strongest in apolar regions of the system and subsides in polar regions, since the polar and apolar contributions to the active stress appear in equation (50) with opposite signs. We plot the magnitude of the active pressure $\Pi^{(A)} \simeq 1 - |\mathbf{P}|^2$ as a function of $|\mathbf{P}|$ in table 2. This is reminiscent of the behavior predicted in the frameworks of a sparsely crosslinked system in [21]. In contrast the effects of non-symmetric motors can be enhanced in polar regions. Consider again, the example of a motor with one static head that preferentially binds near one of the filament ends and a mobile head that acts uniformly. For this motor $\sigma_{10} = \gamma_1 V_0$ and $\sigma_{01} = 0$ and $\sigma_0 = \gamma_0 V_0/2$. It is thus predicted to generate twice the amount of active pressure in a polar network than in an apolar one and $\Pi^{(A)} \simeq (1 + |\mathbf{P}|)/2$, see the table 2 for a plot of the active pressure $\Pi^{(A)}$ as a function of $|\mathbf{P}|$. This is reminiscent of the motor dynein in spindles, which is thought to generate the most prominent contractions near the spindle poles, which are polar [40].

Finally, we ask how filament length affects the active pressure. Looking at the definitions of the nematic and polar activity equations (48) and (52) and remembering the definition and scaling of the coefficient in there (see appendix D), we notice that the active pressure scales as L^4 . Since the viscosity scaled with L^2 , this predicts that systems with shorter filaments contract slower than systems with longer filaments. This effect has been observed for dynein based contractions *in vitro* [20].

5.5. Tuning axial stresses, buckling and aster formation

Motors in active filament networks generate anisotropic (axial) contributions to the stress, which can lead to large scale instabilities in materials with nematic order [3, 26, 36, 41]. At larger active stresses, nematics are unstable to splay deformations in systems that are contractile along the nematic axis, and to bend deformations in systems that are extensile along the nematic axis [7, 36]. In both cases, the instabilities set in when the square root of ratio of the elastic (bend or splay) modulus that opposes the deformation to the active stress—also called the Fréedericksz length—becomes comparable to the systems size. We now discuss which motor properties control the emergence of these instabilities, and how a system can be tuned exhibit bend or splay deformations. For this we ask how axial stresses, which are governed by the activity parameters $\mathcal{A}^{(Q)}$ and $\mathcal{A}^{(P)}$, are set in our system.

The magnitude S of the axial stress along the nematic axis is given by

$$S = -\rho^2 q (\mathcal{A}^{(Q)} - \mathcal{A}^{(P)}|\mathbf{P}|^2), \quad (65)$$

where we defined the nematic order parameter q , as the largest eigenvalue of $\mathcal{Q} - \text{Tr}(\mathcal{Q})\mathcal{I}/3$; see equation (50). The axial stress is contractile along the nematic axis if S is positive and extensile if S is negative. Comparing equations (63) and (65) we find that $S = q(\Pi^{(A)} + \rho^2 \alpha K_0)$ and in the limit where $K_0 \rightarrow 0$, where motor elasticity is negligible, $S = q\Pi^{(A)}$. We discussed how $\Pi^{(A)}$ is set for different types of crosslinks in the previous section; see table 2.

The prototypical active nematic [37] which consists of apolar bundles of microtubules actuated by the kinesin motors and is axial extensile. In our theory, an axial extensile stress (i.e. $S < 0$) in an apolar system ($\mathbf{P} = 0$) implies that $\mathcal{A}^{(Q)} = \sigma_{10} - \sigma_0 \frac{\alpha}{\gamma_0} + \frac{L^2}{12} K_0 > 0$. This can be achieved either by crosslinks that act uniformly (i.e. $\sigma_{10} - \sigma_0 \frac{\alpha}{\gamma_0} = 0$) and generate a spring like response that induces $K_0 > 0$ or by crosslinks

that have non-uniform motor stepping behavior which generates $\sigma_{10} - \sigma_0 \frac{\gamma_1}{\gamma_0} > 0$. The latter implies either a non-symmetric motor crosslinks, or the presence of more than one kind of crosslinks, as was discussed more extensively earlier in the context of active pressure. At high enough active stress we expect systems with negative S to become unstable toward buckling. This has been observed in [42, 43].

Conversely axial contractile behavior can be achieved if either $K_0 < 0$ or $\sigma_{10} - \sigma_0 \frac{\gamma_1}{\gamma_0} < 0$. At high enough active stress, such systems can become unstable toward an aster forming transition, as seen in [38].

Note that $S \simeq \Pi^{(A)} + \rho^2 \alpha K_0$, implies that S and $\Pi^{(A)}$ need not be the same if $K_0 \neq 0$. In particular when $\Pi^{(A)}$ and K_0 have opposite signs systems can exist, which are axially extensible while being bulk contractile and vice versa.

We finally note that the magnitude of axial stresses changes if the system transitions from apolar to polar, if the origin of the axial stresses is motor stepping but not if the origin of the axial stresses is the effective spring like behavior of motor, since $\mathcal{A}^{(Q)}$, but not $\mathcal{A}^{(P)}$, depends on K_0 , see equations (48) and (52). In systems in which the active stress is generated by the stepping of symmetric motor-crosslink, $|S|$ is highest nematic apolar phase ($|\mathbf{P}| = 0$), while systems made from non-symmetric crosslinks generate the most stress when polar ($|\mathbf{P}| = 1$); see table 2. This opens the possibility that a system can overcome the threshold toward an instability when its other dynamics drives it from nematic apolar to polar arrangements or vice versa. We suggest that the buckling instabilities discussed in [42, 43] should be interpreted in this light.

6. Discussion

In this paper, we asked how the properties of motorized crosslinkers that act between the filaments of a highly crosslinked polymer network set the large scale properties of the material.

For this, we first develop a method for quantitatively stating what the properties of motorized crosslinks are. We introduce a generic phenomenological model for the forces that crosslink populations exert between the filaments which they connect; see equation (25). This model describes forces that are (i) proportional to the distance (K), and (ii) the relative rate of displacement (γ). Finally (iii) it describes the active motor forces (σ) that crosslinks can exert. Importantly, forces from crosslinkers (K, γ, σ) can depend on the position on the two filaments which they couple. This allows the description of a wide range of motor properties, such as end-binding affinity, end-dwelling, and even the description of non-symmetric crosslinks that consist of motors with two heads of different properties.

We next derived the stresses and forces generated on large time and length scale, given our phenomenological crosslink model. We find that the emergent material stresses depend only on a small set of moments; see equation (26) of the crosslink properties. These moments are effectively descriptions of the expectation value of the force exerted between two filaments given their positions and relative orientations. The resulting stresses, forces, and filament reorientation rates [equations (46), (49) and (50)] recover the symmetries and structure predicted by phenomenological theories for active materials, but beyond that provide a way of identifying how specific micro-scale processes set specific properties of the material.

We discussed how four key aspects of the dynamics of highly crosslinked filament networks can be tuned by the micro-scale properties of motors and filaments. In particular we discussed how (i) the highly anisotropic viscosity of the material is set; (ii) how active self-straining is regulated; (iii) how contractile or extensible active pressure can be generated; (iv) which motor properties regulate the axial active nematic and bipolar stresses, which can lead to large scale instabilities.

Our theory makes specific predictions for the effects of distinct classes of crosslinkers on cytoskeletal networks. Intriguingly these predictions suggest explanations for phenomena experimentally seen, but currently poorly understood. Experiments have shown that mixtures of actin filaments and myosin molecular motors can spontaneously contract, but only in the presence of an additional passive crosslinker [39]. Our theory allows us to speculate on explanations for this observation. In the crosslink classification that we introduced, myosin, which form large mini-filaments, is a symmetric motor crosslink; see figure (2). We find that symmetric motor crosslinks, which have two heads that act the same can generate contractions only in the presence of an additional crosslinker that helps break the balance between $\gamma_1/\gamma_0\sigma_0$ and σ_{01} in the active pressure; see equation (64) and table 2. Since the addition of passive crosslinks also increases the viscosity of the system, we predict a maximal rate of contraction at an intermediate concentration of passive crosslinks, when the contributions to γ_0 generated by passive and active components are equal. This prediction is qualitatively consistent with ideas presented in [19, 39] but further work will be needed to explore whether this connection can be made quantitative.

A second observation that was poorly understood prior to this work is the sliding motion of microtubules in meiotic *Xenopus* spindles, which are the structures which segregate chromosomes during the meiotic cell division. These spindles consist of inter-penetrating arrays of anti-parallel microtubules,

which are nematic near the chromosomes, and highly polar near the spindle poles. In most of the spindle the two anti-parallel populations of microtubules slide past each other, at near constant speed driven by the molecular motor Eg-5 Kinesin, regardless of the local network polarity. Our earlier work [30] showed that active self straining explains this polarity independent motion. The theory that we develop here provides the tools to explore the behavior of different motors and motor mixtures which will allow us to investigate the mechanism by which different motors in the spindle shape its morphology. This will help to explain complex behaviors of spindles such as the barreling instability [13] that gives spindles their characteristic shape or the observation that spindles can fuse [44].

Our theory provides specific predictions on how changing motor properties can change the properties of the material which they constitute, it can enable the design of new active materials. We predict the expected large scale properties of a material, in which an experimentalist had introduced engineered crosslinks with controlled properties. With current technology, an experimentalist could engineer a motor that preferentially attaches one of its heads to a specified location on a filament, while its walking head reaches out into the network. Or, as has already been demonstrated in studies by the Surrey lab [45] the difference in the rates of filament growth and motor walking speeds, could be exploited to generate different dynamic motor distributions on filaments. This design space will provide ample room to experimentally test our predictions, and use them to engineer systems with desirable properties. Finally recent advances in optical control of motor systems [46] could be used to provide spatial control.

Another way of testing the predictions that we make here, would be to interrogate numerical models using toolboxes such as Cytosim [47] or AMSOS [48]. In simulation, the distribution of crosslinks on filaments, and thus the crosslink moments, can be directly measured. Given these moments, our theory predicts the large scale dynamics of the system, which can then be compared to the actual observed dynamics.

The theory presented here does however makes important simplifications. Importantly, we neglected that the distribution of bound crosslinks on filaments themselves in general depends on the configuration of the network. This means that the crosslink moments can themselves be functions of the local network order parameters. Effects like this have been argued to be important for instance when explaining the transition from contractile to extensile stresses in ordering microtubule networks [49] and the physics of active bundles [28]. Such effects can be recovered when making the interactions K, γ, σ in the phenomenological crosslink force model equation (25) functions of \mathbf{p}_i and \mathbf{p}_j . This will be the topic of a subsequent publication. Furthermore, our theory describes filaments as rigid line segments. This choice neglects effects due to filament elasticity, their finite diameter, and helical microstructure. Actin filaments and microtubules are structurally chiral, which has been shown to induce chiral interactions between motors and filaments [50–52] and conjectured to generate active chiral stresses in the materials that they form [11]. Further work will be needed to incorporate these effects in the framework that we establish here. Finally, we constrain ourselves to a regime of transient crosslinks where we do not allow information to be stored elastically; for an examination of systems where elastic time-scales are important see [29] and references therein.

The model for crosslinker mediated filament–filament interactions that we propose in equation (25), and upon which our theory is based, is a phenomenological description of the forces that molecular scale agents collectively exert between the filaments which they connect. It allows us to categorize populations of crosslinks, as collectively acting as passive or active, symmetric or asymmetric, and uniform or non-uniform. We do however emphasize that our theory makes no predictions on how the coefficients in equation (25) and the crosslink moments that follow, are set by microscopic interactions between molecules on filaments. These interactions can be detailed and complicated and might, on a microscopic level, blur the boundaries between active and passive interactions. For instance, the passive microtubule crosslink Ase1 is known to be actively transported along microtubules by kinesins [53], which is responsible for the non-uniform distribution of Ase1 on microtubules. Thus, the distribution of the passive crosslink is set by an active process. Another example are charged ions which can act as crosslinks, since cytoskeletal filaments in suspension carry charge [54]. Thus they can contribute to the crosslink moments and the potential energy $e(\mathbf{x}_i, \mathbf{p}_i)$ for filament interactions; see appendix F. Studying these and other molecular scale processes goes beyond this work. Ultimately to get a mechanistic handle on how the coefficients in equation (25) are set, more microscopic models in the style of [55] need to be generalized and coarse grained.

Finally, we have ignored interactions of the active gel with the solvent in which it is suspended. In the bulk of a highly crosslinked material this approximation is justified by the fact that the characteristic length over which momentum transport through the gel occurs increases with the square-root of the gel density, while the typical length scale over which momentum is transported through the solvent—the permeation length—decreases with the gel density [30]. However, near the boundaries of an active gel structure immersed in a solvent, the full expressions (given in appendix C) should be used to account for permeation

effects, and the flow of the solvent needs to be solved for. We suspect that poroelastic effects, which result from the interplay of the gel and its solvent are important to understand the physics of large cytoskeletal structures such as microtubule asters [56] and spindles [57].

In summary, in this paper we derived a continuum theory for systems made from cytoskeletal filaments and motors in the highly crosslinked regime. Our theory makes testable predictions on the behavior of the emerging system, provides a unifying framework in which dense cytoskeletal systems can be understood from the ground up, and provides the design paradigms, which will enable the creation of active matter systems with desirable properties in the lab.

Acknowledgments

We thank Meredith Betterton and Adam Lamson for insightful discussions. We also thank Peter J Foster and James F Pelletier for feedback on the manuscript. DN acknowledges support by the National Science Foundation under Awards DMR-2004380, DMR-1420570, DMR-0820484, and PHY-2013874. MJS acknowledges support by the National Science Foundation under Awards Nos. DMR-1420073 (NYU MRSEC), DMS-1620331, and DMR-2004469.

Appendix A. Notation

For clarity we define our notational conventions here, using index notation. We start by defining the generalized outer product between vectors \mathbf{a} , \mathbf{b} , \mathbf{c} , ... as

$$(\mathbf{abc} \dots)_{\alpha\beta\gamma\dots} = a_\alpha b_\beta c_\gamma \dots \quad (\text{A1})$$

and the inner product between vectors as

$$\mathbf{a} \cdot \mathbf{b} = a_\gamma b_\gamma, \quad (\text{A2})$$

where summation over repeated indices is implied. This notation generalizes to tensors. The inner product between the n th rank tensor \mathcal{A} and the m th rank tensor \mathcal{B} is given by

$$(\mathcal{A} \cdot \mathcal{B})_{\alpha_1, \dots, \alpha_{n-1} \beta_1, \dots, \beta_{m-1}} = A_{\alpha_1, \dots, \alpha_{n-1} \gamma} B_{\gamma \beta_1, \dots, \beta_{m-1}}, \quad (\text{A3})$$

and $\mathcal{A} \cdot \mathcal{B}$ is an $m + n - 2$ nd rank tensor.

Finally, we use the shorthand: to denote the contraction

$$(\mathcal{A} : \mathcal{B})_{\alpha_1, \dots, \alpha_{n-2} \beta_1, \dots, \beta_{m-2}} = A_{\alpha_1, \dots, \alpha_{n-2} \mu \gamma} B_{\gamma \mu \beta_1, \dots, \beta_{m-2}}. \quad (\text{A4})$$

Appendix B. Coarse graining distributions into functions

In this paper we often employ distributions. For instance the particle density ψ [see equation (1)] is defined as

$$\psi(\mathbf{x}, \mathbf{p}) = \sum_i \delta(\mathbf{x} - \mathbf{x}_i) \delta(\mathbf{p} - \mathbf{p}_i), \quad (\text{B1})$$

which is a distribution and not a smooth function. From such representations, it is straightforward to construct, or to reinterpret these as, smooth (if short-handed) representations of fields. For simplicity, consider a density of only positional coordinates

$$\psi(\mathbf{x}) = \sum_i \delta(\mathbf{x} - \mathbf{x}_i). \quad (\text{B2})$$

As an example, let $C(|\mathbf{x}|)$ be a nonnegative C^∞ rapidly decaying function of unit mass (and hence having units of inverse volume). The function $\delta_\varepsilon(\mathbf{x}) = \varepsilon^{-3} C(|\mathbf{x}|/\varepsilon)$ is then an approximate δ -function. We define a smooth density through convolution with δ_ε :

$$\Psi(\mathbf{x}) = \int d\mathbf{x}'^3 \delta_\varepsilon(\mathbf{x} - \mathbf{x}') \psi(\mathbf{x}') = \sum_i \delta_\varepsilon(\mathbf{x} - \mathbf{x}_i). \quad (\text{B3})$$

It is easy to check that Ψ again satisfies a Smoluchowski equation like equation (2):

$$\partial_t \Psi + \nabla \cdot (\dot{\mathbf{x}} \Psi) = 0 \quad (\text{B4})$$

where

$$\Psi(\mathbf{x})\dot{\mathbf{x}} = \sum_i \delta_\varepsilon(\mathbf{x} - \mathbf{x}_i)\dot{\mathbf{x}}_i, \quad (\text{B5})$$

in analogy to equations (3) and (4). Upon adding the conformation variable \mathbf{p} , another approximate δ -function upon the unit \mathbf{p} -sphere must be introduced (and so is without dimension), and equation (B2) appropriately modified. One can make various interpretations in moving to smooth fields. One is that the length-scale ε is a coarse-graining scale, much shorter than the system scale but nonetheless capturing many particles within its span (see [20]).

We emphasize that the same line of argument holds for the definitions of all the distributions introduced in the main text, which can trivially be changed into functions by explicitly carrying out a coarse graining step. In the main text we choose to keep working with distributions, for simplicity. For a more exhaustive treatment of coarse graining procedures for polymeric materials we refer the reader to [34].

Appendix C. Derivation of the equations of motion

In the following we derive the equations of motion for the highly crosslinked active network. We start by using equations (24) and (45) and obtain

$$\dot{\mathbf{p}}_i = (\mathcal{I} - \mathbf{p}_i\mathbf{p}_i) \cdot \left\{ \mathbf{p}_i \cdot \left(\mathcal{U} + \frac{12}{\gamma_0 L^2} \frac{\mathcal{E}}{\rho^2} \right) + \frac{12}{\gamma_0 L^2} A^{(\mathbf{P})} \mathbf{P} \right\} - \frac{1}{\rho} \bar{\mathbf{T}}_i^{(\text{drag})}, \quad (\text{C1})$$

The torque due to drag with the medium is

$$\bar{\mathbf{T}}_i^{(\text{drag})} = \mathbf{T}_i^{(\text{drag})} + (\mathcal{I} - \mathbf{p}_i\mathbf{p}_i) \cdot \left(\frac{12}{\gamma_0 L^2} + \mathbf{p}_i \cdot \frac{\nabla \rho}{\rho} \right) \left(\mathbf{F}_i^{(\text{drag})} - \frac{1}{\rho} \mathbf{f} \right). \quad (\text{C2})$$

This implies

$$\omega = \mathbf{P} \cdot \left(\mathcal{U} + \frac{12}{\gamma_0 L^2} \frac{\mathcal{E}}{\rho^2} \right) - \mathcal{T} : \left(\mathcal{U} + \frac{12}{\gamma_0 L^2} \frac{\mathcal{E}}{\rho^2} \right) + \frac{12}{L^2} A^{(\mathbf{P})} (\mathbf{P} - \mathcal{Q} \cdot \mathbf{P}) - \frac{1}{\rho} \omega^{(\text{drag})}, \quad (\text{C3})$$

where

$$\omega^{(\text{drag})} = \left\langle \bar{\mathbf{T}}_i^{(\text{drag})} \right\rangle \quad (\text{C4})$$

and

$$\mathcal{H} = \mathcal{Q} \cdot \left(\mathcal{U} + \frac{12}{\gamma_0 L^2} \frac{\mathcal{E}}{\rho^2} \right) - \mathcal{S} : \left(\mathcal{U} + \frac{12}{\gamma_0 L^2} \frac{\mathcal{E}}{\rho^2} \right) + \frac{12}{\gamma_0 L^2} A^{(\mathbf{P})} (\mathbf{P}\mathbf{P} - \mathcal{T} \cdot \mathbf{P}) - \frac{1}{\rho} \mathcal{H}^{(\text{drag})}, \quad (\text{C5})$$

where

$$\mathcal{H}^{(\text{drag})} = \left\langle \mathbf{p}_i \bar{\mathbf{T}}_i^{(\text{drag})} \right\rangle. \quad (\text{C6})$$

Furthermore we note that

$$\mathbf{j} = \frac{\sigma_0}{\gamma_0} (\mathbf{P}\mathbf{P} - \mathcal{Q}) + \frac{1}{\gamma_0 \rho} \mathbf{j}^{(\text{drag})} + \mathcal{O}(L^2), \quad (\text{C7})$$

and

$$\mathcal{J} = \frac{\sigma_0}{\gamma_0} (\mathcal{Q}\mathbf{P} - \mathcal{T}) + \frac{1}{\gamma_0 \rho} \mathcal{J}^{(\text{drag})} + \mathcal{O}(L^2), \quad (\text{C8})$$

where

$$\mathbf{j}^{(\text{drag})} = -\frac{1}{\gamma_0} \left\langle \mathbf{p}_i \left(\mathbf{F}_i^{(\text{drag})} - \frac{1}{\rho} \mathbf{f} \right) \right\rangle \quad (\text{C9})$$

and

$$\mathcal{J}^{(\text{drag})} = -\frac{1}{\gamma_0} \left\langle \mathbf{p}_i \mathbf{p}_i \left(\mathbf{F}_i^{(\text{drag})} - \frac{1}{\rho} \mathbf{f} \right) \right\rangle. \quad (\text{C10})$$

Putting all of this together, we arrive at an expression for the networks stress in terms of the current distribution of filaments,

$$\Sigma = -\rho^2 (\chi : \mathcal{U} + \alpha K_0 \mathcal{I}) - \rho^2 (A^{(\mathcal{Q})} \mathcal{Q} - A^{(\mathbf{P})} \mathcal{T} \cdot \mathbf{P}) - \bar{\chi} : \mathcal{E} + \bar{\Sigma} + \rho \Sigma^{(\text{drag})}. \quad (\text{C11})$$

where

$$\Sigma^{(\text{drag})} = -\gamma_0 \frac{L^2}{12} \mathcal{H}^{(\text{drag})} - \gamma_1 \mathbf{j}^{(\text{drag})} \quad (\text{C12})$$

and at a similar equation for the motion of filament i

$$\begin{aligned}
\mathbf{v}_i - \mathbf{v} = & -\frac{\sigma_0}{\gamma_0} (\mathbf{p}_i - \mathbf{P}) \\
& - \frac{\gamma_1}{\gamma_0} \left(\begin{aligned} & (\mathbf{p}_i - \mathbf{P}) \cdot \left(\mathcal{U} + \frac{12}{\gamma_0 L^2} \frac{\mathcal{E}}{\rho^2} \right) \\ & - (\mathbf{p}_i \mathbf{p}_i \mathbf{p}_i - \mathcal{T}) : \left(\mathcal{U} + \frac{12}{\gamma_0 L^2} \frac{\mathcal{E}}{\rho^2} \right) \end{aligned} \right) \\
& + \frac{1}{\gamma_0} \frac{12\gamma_1}{L^2\gamma_0} A^{(\mathbf{P})} (\mathbf{p}_i \mathbf{p}_i - \mathcal{Q}) \cdot \mathbf{P} \\
& - \frac{\nabla \rho}{\gamma_0 \rho} \cdot \left[\begin{aligned} & A^{(\mathcal{Q})} (\mathbf{p}_i \mathbf{p}_i - \mathcal{Q}) \\ & - A^{(\mathbf{P})} (\mathbf{p}_i \mathbf{P} + \mathbf{P} \mathbf{p}_i - 2\mathbf{P}\mathbf{P}) \end{aligned} \right] \\
& - \left(\mathbf{p}_i \mathbf{p}_i - \mathcal{Q} \right) : \nabla \frac{\mathcal{E}}{\rho} - \frac{1}{\rho} \mathbf{v}^{(\text{drag})} \tag{C13}
\end{aligned}$$

where

$$\frac{1}{\rho} \mathbf{v}^{(\text{drag})} = \frac{1}{\rho\gamma_0} \mathbf{F}_i^{(\text{drag})} + \mathcal{O}(1/\rho^2). \tag{C14}$$

In the main text of this paper we chose to ignore drag-effects, which in general come from the interactions between that cytoskeletal network and the solvent in which it is submerged, for simplicity and because their relative importance diminishes quadratically as ρ increases. At lower densities however, they can become important, and in more dilute suspensions they can even dominate the long range momentum transport. This case has been treated in [24, 26] and others.

Appendix D. Crosslink moments and generalization to variable filament lengths

The crosslink moment which enter the hydrodynamic descriptions are defined from moments of crosslinker mediated filament–filament forces. Specifically,

$$K_0 = [K(s_i, s_j)]_{\Omega(\mathbf{x}_i)}^{ij}, \tag{D1}$$

$$K_1 = [s_i K(s_i, s_j)]_{\Omega(\mathbf{x}_i)}^{ij}, \tag{D2}$$

$$\gamma_0 = [\gamma(s_i, s_j)]_{\Omega(\mathbf{x}_i)}^{ij}, \tag{D3}$$

$$\gamma_1 = [s_i \gamma(s_i, s_j)]_{\Omega(\mathbf{x}_i)}^{ij}, \tag{D4}$$

$$\sigma_0 = [\sigma(s_i, s_j)]_{\Omega(\mathbf{x}_i)}^{ij}, \tag{D5}$$

$$\sigma_{10} = [s_i \sigma(s_i, s_j)]_{\Omega(\mathbf{x}_i)}^{ij}, \tag{D6}$$

and

$$\sigma_{01} = [s_j \sigma(s_i, s_j)]_{\Omega(\mathbf{x}_i)}^{ij}. \tag{D7}$$

In the main text, for simplicity, we constrained ourselves to the case of filaments which all have the same length L . It is however straightforward to generalize the definition of the operator $[\dots]_{\Omega(\mathbf{x})}^{ij}$ to treat variable length filament distributions. To describe variable length filaments, we redefine $[\dots]_{\Omega(\mathbf{x})}^{ij}$ in equation (19) as

$$\begin{aligned}
[\phi]_{\Omega(\mathbf{x}_i)}^{ij} &= \int_{-\frac{L_i}{2}}^{\frac{L_i}{2}} ds_i \int_{-\frac{L_j}{2}}^{\frac{L_j}{2}} ds_j \int_{\Omega(\mathbf{x}_i)} d\mathbf{x}^3 \phi(s_i/L_i, s_j/L_i) \\
&= L_i L_j \int_{-\frac{1}{2}}^{\frac{1}{2}} d\hat{s}_i \int_{-\frac{1}{2}}^{\frac{1}{2}} d\hat{s}_j \int_{\Omega(\mathbf{x}_i)} d\mathbf{x}^3 \phi(\hat{s}_i, \hat{s}_j), \tag{D8}
\end{aligned}$$

where $L_i \hat{s}_i = s_i$ and $L_j \hat{s}_j = s_j$. Under this redefinition the crosslink moments from equation (26) become

$$X_{mm}^{ij}(\mathbf{x}) = [X(\hat{s}_i, \hat{s}_j) \hat{s}_i^n \hat{s}_j^m]_{\Omega(\mathbf{x})}^{ij}. \tag{D9}$$

All calculations in the main text can be carried through with this redefinition.

Appendix E. Angular momentum fluxes and antisymmetric stresses

The spin and orbital angular momenta obey the continuity equations

$$\dot{\ell}_i = \sum_j \mathbf{T}_{ij} + \mathbf{T}_i^{(\text{drag})} \quad (\text{E1})$$

and

$$\mathbf{x}_i \times \dot{\mathbf{g}}_i = \sum_j \mathbf{x}_i \times \mathbf{F}_{ij} + \mathbf{x}_i \times \mathbf{F}_i^{(\text{drag})}, \quad (\text{E2})$$

where we used equation (5) and that $\dot{\mathbf{x}}_i$ is parallel to \mathbf{g} . We and introduce the densities of spin and orbital angular momentum which are

$$\ell = \sum_i \delta(\mathbf{x} - \mathbf{x}_i) \ell_i, \quad (\text{E3})$$

and

$$\ell^{(\text{orb})} = \sum_i \delta(\mathbf{x} - \mathbf{x}_i) \mathbf{x}_i \times \mathbf{g}_i, \quad (\text{E4})$$

respectively. They obey continuity equations

$$\partial_t \ell + \nabla \cdot \sum_i (\delta(\mathbf{x} - \mathbf{x}_i) \mathbf{v}_i \ell_i) = \sum_{ij} \delta(\mathbf{x} - \mathbf{x}_i) \mathbf{T}_{ij} + \tau, \quad (\text{E5})$$

where

$$\tau = \sum_i \delta(\mathbf{x} - \mathbf{x}_i) \mathbf{T}_i^{(\text{drag})} \quad (\text{E6})$$

and

$$\partial_t \ell^{(\text{orb})} + \nabla \cdot \sum_i \delta(\mathbf{x} - \mathbf{x}_i) \mathbf{v}_i \mathbf{x}_i \times \mathbf{g}_i = \sum_{ij} \delta(\mathbf{x} - \mathbf{x}_i) \mathbf{x}_i \times \mathbf{F}_{ij} + \mathbf{x} \times \mathbf{f}. \quad (\text{E7})$$

The first term on the right-hand side of equation (E7) describes the orbital angular momentum transfer by crosslink interactions. It can be rewritten as the sum of an orbital angular momentum flux $\mathcal{M}^{(\text{orb})}$ and a source term related to the antisymmetric part of the stress tensor Σ ,

$$\begin{aligned} & \sum_{ij} \delta(\mathbf{x} - \mathbf{x}_i) \mathbf{x}_i \times \mathbf{F}_{ij} \\ &= \sum_{ij} \delta(\mathbf{x} - \mathbf{x}_i) \frac{\mathbf{x}_i + \mathbf{x}_j}{2} \times \mathbf{F}_{ij} + \sum_{ij} \delta(\mathbf{x} - \mathbf{x}_i) \frac{\mathbf{x}_i - \mathbf{x}_j}{2} \times \mathbf{F}_{ij} \\ &= \nabla \cdot \mathcal{M}^{(\text{orb})} + 2\sigma^a + \mathcal{O}(\mathbf{d}_{ij}^3), \end{aligned} \quad (\text{E8})$$

where the orbital angular momentum flux is

$$\mathcal{M}^{(\text{orb})} = - \sum_{ij} \delta(\mathbf{x} - \mathbf{x}_i) \frac{\mathbf{x}_i - \mathbf{x}_j}{2} \left(\frac{\mathbf{x}_i + \mathbf{x}_j}{2} \times \mathbf{F}_{ij} \right) \quad (\text{E9})$$

and

$$\sigma^a = \sum_{ij} \delta(\mathbf{x} - \mathbf{x}_i) \frac{\mathbf{x}_i - \mathbf{x}_j}{4} \times \mathbf{F}_{ij}, \quad (\text{E10})$$

which is the pseudo-vector notation for the antisymmetric part of the stress Σ such that in index notation,

$$\sigma_\alpha^a = \frac{1}{2} \epsilon_{\alpha\beta\gamma} \Sigma_{\beta\gamma}, \quad (\text{E11})$$

where used the Levi-Civita symbol $\epsilon_{\alpha\beta\gamma}$ and summation over repeated greek indices is implied.

Similarly, the first term on the right-hand side of equation (E5) describes the spin angular momentum transfer by crosslink interactions. It can be rewritten as the sum of an orbital angular momentum flux \mathcal{M} and a source term related to the antisymmetric part of the stress tensor Σ ,

$$\begin{aligned}
& \sum_{ij} \delta(\mathbf{x} - \mathbf{x}_i) \mathbf{T}_{ij} \\
&= \sum_{ij} \delta(\mathbf{x} - \mathbf{x}_i) \left(\mathbf{T}_{ij} + \frac{\mathbf{x}_i - \mathbf{x}_j}{2} \times \mathbf{F}_{ij} \right) - \sum_{ij} \delta(\mathbf{x} - \mathbf{x}_i) \frac{\mathbf{x}_i - \mathbf{x}_j}{2} \times \mathbf{F}_{ij} \\
&= \nabla \cdot \mathcal{M} - 2\sigma^a + \mathcal{O}(\mathbf{d}_{ij}^3),
\end{aligned} \tag{E12}$$

where the spin angular momentum flux

$$\mathcal{M} = - \sum_{ij} \delta(\mathbf{x} - \mathbf{x}_i) \frac{\mathbf{x}_i - \mathbf{x}_j}{2} \left(\mathbf{T}_{ij} + \frac{\mathbf{x}_i - \mathbf{x}_j}{2} \times \mathbf{F}_{ij} \right). \tag{E13}$$

After defining the total and spin angular momentum fluxes as

$$\mathcal{M}^{(\text{tot})} = \mathcal{M} + \mathcal{M}^{(\text{orb})} = - \sum_{ij} \delta(\mathbf{x} - \mathbf{x}_i) \frac{\mathbf{x}_i - \mathbf{x}_j}{2} (\mathbf{T}_{ij} + \mathbf{x}_i \times \mathbf{F}_{ij}), \tag{E14}$$

we finally write down the statements of angular momentum conservation

$$\nabla \cdot \mathcal{M}^{(\text{tot})} + \mathbf{x} \times \mathbf{f} + \tau = 0, \tag{E15}$$

spin angular momentum continuity

$$\nabla \cdot \mathcal{M} - 2\sigma^a + \tau = 0, \tag{E16}$$

and orbital angular momentum continuity

$$\nabla \cdot \mathcal{M}^{(\text{orb})} + 2\sigma^a + \mathbf{x} \times \mathbf{f} = 0, \tag{E17}$$

where we dropped inertial terms. We note that the antisymmetric stress Σ^a acts to transfer spin to orbital angular momentum. Importantly, the total angular momentum is conserved as evident from the form of equation (E15).

Appendix F. The Ericksen stress

In this appendix we derive the effects of steric interactions on the system. As stated in the main text, steric interactions are best described in terms of a potential $e(\mathbf{x}_i, \mathbf{p}_i)$, which depends on all particle positions and orientations. The steric free energy of the system is $E = \int_{\mathcal{V}} e \, d^3x$ where \mathcal{V} is the volume of the system. For the treatment to follow we shall assume the steric interactions do not depend on the polar, but only on the nematic order of the system. Then a generic variation of the systems free energy can be written as

$$\delta E = \int_{\partial\mathcal{V}} \left(e u_\gamma + \frac{\partial e}{\partial(\partial_\gamma Q_{\alpha\beta})} \delta Q_{\alpha\beta} \right) dS_\gamma - \int_{\partial\mathcal{V}} (\mu \delta \rho + \mathcal{E}_{\alpha\beta} \delta Q_{\alpha\beta}) \tag{F1}$$

where we defined the chemical potential

$$\mu = - \frac{\partial e}{\partial \rho} \tag{F2}$$

and the distortion field

$$\mathcal{E}_{\alpha\beta} = - \frac{\partial e}{\partial Q_{\alpha\beta}} + \partial_\gamma \frac{\partial e}{\partial(\partial_\gamma Q_{\alpha\beta})}, \tag{F3}$$

and introduced the infinitesimal deformation field \mathbf{u} . Now, any physically well defined free energy density needs to obey translation invariance. Thus $\delta E = 0$ for any pure translation, which is the transformation where $\delta \rho = -u_\gamma \partial_\gamma \rho$, $\delta Q_{\alpha\beta} = -u_\gamma \partial_\gamma Q_{\alpha\beta}$, u_γ is a constant. Thus

$$\partial_\beta \left((e + Q_{\mu\nu} \mathcal{E}_{\mu\nu} + \mu \rho) \delta_{\alpha\beta} - \frac{\partial e}{\partial(\partial_\beta Q_{\gamma\mu})} \partial_\alpha Q_{\gamma\mu} \right) = \rho \partial_\alpha \mu + Q_{\mu\nu} \partial_\alpha \mathcal{E}_{\mu\nu}, \tag{F4}$$

which is the Gibbs–Duhem relation used in the main text, where

$$\bar{\Sigma}_{\alpha\beta} = (e + Q_{\mu\nu} \mathcal{E}_{\mu\nu} + \mu \rho) \delta_{\alpha\beta} - \frac{\partial e}{\partial(\partial_\beta Q_{\gamma\mu})} \partial_\alpha Q_{\gamma\mu}. \tag{F5}$$

ORCID iDs

Sebastian Fürthauer  <https://orcid.org/0000-0001-9581-5963>

Michael J Shelley  <https://orcid.org/0000-0002-4835-0339>

References

- [1] Bois J S, Jülicher F and Grill S W 2011 Pattern formation in active fluids *Phys. Rev. Lett.* **106** 028103
- [2] Voituriez R, Joanny J F and Prost J 2005 Spontaneous flow transition in active polar gels *Europhys. Lett.* **70** 404
- [3] Fürthauer S, Neef M, Grill S W, Kruse K and Jülicher F 2012 The Taylor–Couette motor: spontaneous flows of active polar fluids between two coaxial cylinders *New J. Phys.* **14** 023001
- [4] Wioland H, Woodhouse F G, Dunkel J, Kessler J O and Goldstein R E 2013 Confinement stabilizes a bacterial suspension into a spiral vortex *Phys. Rev. Lett.* **110** 268102
- [5] Salbreux G, Prost J and Joanny J-F 2009 Hydrodynamics of cellular cortical flows and the formation of contractile rings *Phys. Rev. Lett.* **103** 058102
- [6] Brugués J and Needleman D 2014 Physical basis of spindle self-organization *Proc. Natl Acad. Sci. USA* **111** 18496–500
- [7] Marchetti M C, Joanny J F, Ramaswamy S, Liverpool T B, Prost J, Rao M and Simha R A 2013 Hydrodynamics of soft active matter *Rev. Mod. Phys.* **85** 1143
- [8] Alberts B, Bray D, Lewis J, Raff M, Roberts K and Watson J D 2002 *Molecular Biology of the Cell* 4th edn (New York: Garland)
- [9] Howard J et al 2001 *Mechanics of Motor Proteins and the Cytoskeleton* (Sunderland, MA: Sinauer Associates)
- [10] Kruse K, Joanny J-F, Jülicher F, Prost J and Sekimoto K 2004 Asters, vortices, and rotating spirals in active gels of polar filaments *Phys. Rev. Lett.* **92** 078101
- [11] Fürthauer S, Stempel M, Grill S W and Jülicher F 2012 Active chiral fluids *Eur. Phys. J. E* **35** 89
- [12] Jülicher F, Grill S W and Salbreux G 2018 Hydrodynamic theory of active matter *Rep. Prog. Phys.* **81** 076601
- [13] Oriola D, Jülicher F and Brugués J 2020 Active forces shape the metaphase spindle through a mechanical instability *Proc. Natl Acad. Sci. USA* **117** 16154–9
- [14] Mayer M, Depken M, Bois J S, Jülicher F and Grill S W 2010 Anisotropies in cortical tension reveal the physical basis of polarizing cortical flows *Nature* **467** 617–21
- [15] Salbreux G, Charas G and Paluch E 2012 Actin cortex mechanics and cellular morphogenesis *Trends Cell Biol.* **22** 536–45
- [16] Naganathan S R, Fürthauer S, Nishikawa M, Jülicher F and Grill S W 2014 Active torque generation by the actomyosin cell cortex drives left-right symmetry breaking *eLife* **3** e04165
- [17] Ram Naganathan S, Fürthauer S, Rodriguez J, Fievet B T, Jülicher F, Ahringer J, Cannistraci C V and Grill S W 2018 Morphogenetic degeneracies in the actomyosin cortex *eLife* **7** e37677
- [18] Foster P J, Fürthauer S, Shelley M J and Needleman D J 2019 From cytoskeletal assemblies to living materials *Curr. Opin. Cell Biol.* **56** 109–14
- [19] Belmonte J M, Leptin M and Nédélec F 2017 A theory that predicts behaviors of disordered cytoskeletal networks *Mol. Syst. Biol.* **13** 941
- [20] Foster P J, Yan W, Fürthauer S, Shelley M J and Needleman D J 2017 Connecting macroscopic dynamics with microscopic properties in active microtubule network contraction *New J. Phys.* **19** 125011
- [21] Gao T, Blackwell R, Glaser M A, Betterton M D and Shelley M J 2015 Multiscale polar theory of microtubule and motor-protein assemblies *Phys. Rev. Lett.* **114** 048101
- [22] Liverpool T B and Marchetti M C 2003 Instabilities of isotropic solutions of active polar filaments *Phys. Rev. Lett.* **90** 138102
- [23] Liverpool T B and Marchetti M C 2005 Bridging the microscopic and the hydrodynamic in active filament solutions *Europhys. Lett.* **69** 846
- [24] Liverpool T B and Marchetti M C 2008 Hydrodynamics and rheology of active polar filaments *Cell Motility* (Berlin: Springer) pp 177–206
- [25] Aranson I S and Tsimring L S 2005 Pattern formation of microtubules and motors: inelastic interaction of polar rods *Phys. Rev. E* **71** 050901
- [26] Saintillan D and Shelley M J 2008 Instabilities and pattern formation in active particle suspensions: kinetic theory and continuum simulations *Phys. Rev. Lett.* **100** 178103
- [27] Kruse K and Jülicher F 2000 Actively contracting bundles of polar filaments *Phys. Rev. Lett.* **85** 1778
- [28] Kruse K and Jülicher F 2003 Self-organization and mechanical properties of active filament bundles *Phys. Rev. E* **67** 051913
- [29] Broeders C P and MacKintosh F C 2014 Modeling semiflexible polymer networks *Rev. Mod. Phys.* **86** 995
- [30] Fürthauer S, Lemma B, Foster P J, Ems-McClung S C, Yu C-H, Walczak C E, Dogic Z, Needleman D J and Needleman M J 2019 Self-straining of actively crosslinked microtubule networks *Nat. Phys.* **15** 1295–300
- [31] Striebel M, Graf I R and Frey E 2020 A mechanistic view of collective filament motion in active nematic networks *Biophys. J.* **118** 313–24
- [32] Martin P C, Parodi O and Pershan P S 1972 Unified hydrodynamic theory for crystals, liquid crystals, and normal fluids *Phys. Rev. A* **6** 2401
- [33] Chaikin P M and Lubensky T C 2000 *Principles of Condensed Matter Physics* (Cambridge: Cambridge University Press)
- [34] Doi M and Edwards S F 1988 *The Theory of Polymer Dynamics* vol 73 (Oxford: Oxford University Press)
- [35] De Gennes P-G and Prost J 1993 *The Physics of Liquid Crystals* vol 83 (Oxford: Oxford University press)
- [36] Kruse K, Joanny J F, Jülicher F, Prost J and Sekimoto K 2005 Generic theory of active polar gels: a paradigm for cytoskeletal dynamics *Eur. Phys. J. E* **16** 5–16
- [37] Sanchez T, Chen D T N, DeCamp S J, Heymann M and Dogic Z 2012 Spontaneous motion in hierarchically assembled active matter *Nature* **491** 431–4
- [38] Foster P J, Fürthauer S, Shelley M J and Needleman D J 2015 Active contraction of microtubule networks *eLife* **4** e10837
- [39] Ennomani H, Letort G, Guérin C, Martiel J-L, Cao W, Nédélec F, De LaCruz E M, Théry M and Blanchoin L 2016 Architecture and connectivity govern actin network contractility *Curr. Biol.* **26** 616–26
- [40] Brugués J, Nuzzo V, Mazur E and Needleman D J 2012 Nucleation and transport organize microtubules in metaphase spindles *Cell* **149** 554–64

- [41] Aditi Simha R and Ramaswamy S 2002 Hydrodynamic fluctuations and instabilities in ordered suspensions of self-propelled particles *Phys. Rev. Lett.* **89** 058101
- [42] Senoussi A, Kashida S, Voituriez R, Galas J-C, Maitra A and Estevez-Torres A 2019 Tunable corrugated patterns in an active nematic sheet *Proc. Natl Acad. Sci. USA* **116** 22464–70
- [43] Strübing T, Khosravanizadeh A, Vilfan A, Bodenschatz E, Golestanian R and Guido I 2019 Wrinkling instability in 3d active nematics (arXiv:1908.10974)
- [44] Gatlin J C, Matov A, Groen A C, Needleman D J, Maresca T J, Danuser G, Mitchison T J and Salmon E D 2009 Spindle fusion requires dynein-mediated sliding of oppositely oriented microtubules *Curr. Biol.* **19** 287–96
- [45] Roostalu J, Rickman J, Thomas C, Nédélec F and Surrey T 2018 Determinants of polar versus nematic organization in networks of dynamic microtubules and mitotic motors *Cell* **175** 796–808
- [46] Ross T D, Lee H J, Qu Z, Banks R A, Phillips R and Thomson M 2019 Controlling organization and forces in active matter through optically defined boundaries *Nature* **572** 224–9
- [47] Sedwards S and Mazza T 2007 Cyto-sim: a formal language model and stochastic simulator of membrane-enclosed biochemical processes *Bioinformatics* **23** 2800–2
- [48] Wen Y, Corona E, Malhotra D, Veerapaneni S and Shelley M 2020 A scalable computational platform for particulate Stokes suspensions *J. Comput. Phys.* **416** 109524
- [49] Martin L 2020 Reversal of contractility as a signature of self-organization in cytoskeletal bundles *eLife* **9** e51751
- [50] Nishizaka T, Yagi T, Tanaka Y and Ishiwata S. i. 1993 Right-handed rotation of an actin filament in an *in vitro* motile system *Nature* **361** 269–71
- [51] Yajima J, Mizutani K and Nishizaka T 2008 A torque component present in mitotic kinesin eg5 revealed by three-dimensional tracking *Nat. Struct. Mol. Biol.* **15** 1119–21
- [52] Mitra A, Meißner L, Gandhimathi R, Renger R, Ruhn F and Diez S 2020 Kinesin-14 motors drive a right-handed helical motion of antiparallel microtubules around each other *Nat. Commun.* **11** 2565
- [53] Lera-Ramirez M and Nédélec F J 2019 Theory of antiparallel microtubule overlap stabilization by motors and diffusible crosslinkers *Cytoskeleton* **76** 600–10
- [54] Boroudjerdi H, Kim Y, Naji A, Netz R, Schlagberger X and Serr A 2005 Statics and dynamics of strongly charged soft matter *Phys. Rep.* **416** 129–99
- [55] Lamson A R, Moore J M, Fang F, Glaser M A, Shelley M and Betterton M D 2020 Comparison of explicit and mean-field models of cytoskeletal filaments with crosslinking motors (arXiv:2011.08156)
- [56] Pelletier J F, Field C M, Fürthauer S, Sonnett M and Mitchison T J 2020 Co-movement of astral microtubules, organelles and f-actin suggests aster positioning by surface forces in frog eggs *eLife* **9** e60047
- [57] Nazockdast E, Rahimian A, Needleman D and Shelley M 2017 Cytoplasmic flows as signatures for the mechanics of mitotic positioning *Mol. Biol. Cell* **28** 3261–70